Middle Holocene marine flooding and human response in the south Yangtze coastal plain, East China

Zhanghua Wang[1*], David B. Ryves[2], Shao Lei[3], Xiaomei Nian[1], Ye Lv[1], Liang Tang[1], Long Wang[1], Jiehua Wang[3], Jie Chen[4]

[1]State Key Laboratory of Estuarine and Coastal Research, East China Normal University, Shanghai 200062, China.

[2]Centre for Hydrological and Ecosystem Science (CHES), Department of Geography, Loughborough University, Loughborough LE11 3TU, UK.

[3]Ningbo Municipal Institute of Cultural Relics and Archaeology, Ningbo 315000, China.

[4]Shanghai Museum, Shanghai 200003, China

*Corresponding author: zhwang@geo.ecnu.edu.cn

Abstract: Coastal flooding catastrophes have affected human societies on coastal plains around the world on several occasions in the past, and are threatening 21st century societies under global warming and sea-level rise. However, the role of coastal flooding in the interruption of the Neolithic Liangzhu culture in the lower Yangtze valley, East China coast has been long contested. In this study, we used a well-dated Neolithic site (the Yushan site) close to the present coastline to demonstrate a marine drowning event at the terminal stage of the Liangzhu culture and discuss its linkage to relative sea-level rise. We analysed sedimentology, chronology, organic elemental composition, diatoms and dinoflagellate cysts for several typical profiles at the Yushan site. The field and sedimentary data provided clear evidence of a palaeo-typhoon event that overwhelmed the Yushan site at ~2560 BCE, which heralded a period of marine inundation and ecological deterioration at the site. We also infer an acceleration in sea-level rise at 2560–2440 BCE from the sedimentary records at Yushan, which explains the widespread signatures of coastal flooding across the south Yangtze coastal plain at that time. The timing of this mid-Holocene coastal flooding coincided with the sudden disappearance of the advanced and widespread Liangzhu culture along the lower Yangtze valley. We infer that extreme events and flooding accompanying accelerated sea-level rise were major causes of vulnerability for prehistoric coastal societies.

Keywords: Palaeo-typhoon event; Sea-level rise; Coastal flooding; Neolithic

1. Introduction

Global sea-level rise is predicted to accelerate during the 21st century and could rise 65±12 cm by 2100 compared with 2005 (Kopp et al., 2016; Nerem et al., 2018), which will increase the frequency of extreme events and the risk of coastal flooding (Woodruff et al., 2013). The vulnerability of low-lying coastal plains and deltas across the world is further exacerbated due to human-induced sediment starvation and land sinking (Syvitski et al., 2009; Giosan et al., 2014). The west Pacific Ocean coast is one of the most vulnerable regions in the world because it is characterized by active tropical cyclones (Woodruff et al., 2013) and, in recent decades, its rate of relative sea-level rise is three times higher than the global mean (Nicholls and Cazenave, 2010). In the densely-populated Yangtze delta, East China (Fig. 1), models under future climate scenarios predict an increase in flood risk from extreme events and relative sea-level rise by 150% to 400% in the next 50 years (Tessler et al., 2015). In fact, Typhoon Fitow (the strongest October typhoon making landfall in China for over 60 years) in 2013 caused flooding to a depth >0.5 m across most of the Yaojiang Plain, south east of the Hangzhou Bay (Fig. 1C). There is thus clearly an urgent need for integrated research on sea-level rise, extreme events, coastal flooding and human response.

Coastal flooding is not a new threat. The fact that the south Yangtze coastal plains (Fig. 1B) hold relative thick and rich archaeological records, preserved in marine and deltaic flood basin sediments (Zong et al., 2007; Zheng et al., 2012), is direct witness of past flooding of these areas during human occupation. Neolithic people including the well-known Kuahuqiao, Hemudu and Liangzhu cultures settled and practiced flood management on the coastal wetlands of Hangzhou Bay (Fig. 1) since ~6000 BCE (Zhao, 1998; Zong et al., 2007; Liu and Chen, 2012; Qin, 2013; Liu et al., 2017). People of the Liangzhu culture, which was one of the most developed and complex societies known in prehistory (Lawler, 2009; Liu and Chen, 2012; Qin, 2013), even constructed massive earth-and-stone walls to hold back floods near their capital city, Mojiaoshan, at the head of Hangzhou Bay near present-day Hangzhou (Fig. 1B; Lawler, 2009; Liu and Chen, 2012; Liu et al., 2017). Yet they abandoned their state capital complex at around 2500 BCE, as shown by dating sedimentary profiles from the capital city (Zhang et al., 2015; Wang et al., 2017), despite their highly developed techniques in agricultural and landscape management (Zhuang et al., 2014; Liu et al., 2017). The subsequent Neolithic Qianshanyang and Guangfulin cultures that appeared at ~2400–1800 BCE were reported to be much less organized and less developed (Shanghai Museum, 2002; ZPICRA and Huzhou Museum, 2014). Studying these archaeological records with a focus on the linkage between flood deposits and cultural interruptions can shed light on the increasing flood risk in this economically important and populous area in the near future.

There has been much speculation and debate surrounding the Liangzhu cultural decline among archaeologists and environmental scientists. Archaeologists speculate that the abandonment of the Liangzhu capital city might have been related to floods because a layer of silt, inferred as flood deposits, was found on top of the late Liangzhu cultural layer in many areas around the capital city (Liu and Chen, 2012). An early environmental study suggested marine inundation played a key role, based on the marine fossil record of core ZX-1 in the eastern Taihu Plain (Stanley et al., 1999), but later work reported no marine flooding at other sites in the Taihu Plain at this time (Zong et al., 2011). Later Innes et al. (2014) suggested a combination of rising local water level and climatic deterioration was the probable cause. We propose that to settle the debate and test these competing hypotheses, it is necessary to carry out an integrated study of relative sea-level change and environmental and human response. It is particularly important to examine directly the event-character of the floodbeds covering the Liangzhu culture layer recovered from archaeological sites.

The Yushan archaeological site was discovered in 2013. It is only 7.3 km from the present coastline (Figs 1, 2A). Diagnostic black pottery and tools for woodworking and farming (Fig. 1D–F) of the Liangzhu culture were recovered from this site. The Liangzhu cultural layer was overlain by mud deposits ~0.4–0.5 m thick which did not contain artefacts, hinting at an inundation event at the end of the Liangzhu culture. Yushan may therefore be key to addressing this debate based on a detailed investigation of the stratigraphic records within this site and may provide important evidence on the mechanisms involved in the decline of the Liangzhu culture. In this study we first carried out multiproxy lithological, sedimentological, palaeontological and organic geochemical analyses of well-dated, high-resolution sequences at multiple locations within the Yushan site to examine the nature of flood deposits covering the Liangzhu cultural layer. We then determined the relative sea level change at the end of the Liangzhu culture using sea level indicators, including the basal peat (Shennan et al., 2015) obtained from the Yushan site. We also synthesised existing profiles from both the Taihu Plain and plains along Hangzhou Bay to compare the flood signatures and to discuss the linkage between relative sea-level rise and flood hazards at the late stage of the Neolithic period on the south Yangtze coast, East China. The results help to resolve this debate over the Liangzhu cultural decline and marine flooding and show the sensitivity and vulnerability of prehistorical human societies to extreme events and flooding.

2. The study area and the site

The south Yangtze coastal plain is mainly made up of the Taihu Plain and coastal plains along the Hangzhou Bay, including the Yaojiang Plain, which is located to the south east and is separated by uplands from Hangzhou Bay (Fig. 1B). Sediments deposited in these plains were derived mainly from the Yangtze River during the Holocene, as sediment load from other local rivers is negligible compared to that from the Yangtze River (Liu et al., 2013). The freshwater-dominated Taihu Plain was formed ~6500–6000 years ago when sea level was relatively stable and the Yangtze delta started its progradation (Hori et al., 2001; Wang et al., 2012). However, the rate of shoreline advance was extremely slow between 6500 and 4000 years ago, as indicated by distribution of the chenier ridges in the east part of the plain (Fig. 1B; Yan et al., 1989), caused mainly by a large amount of sediment trapping in the north Yangtze delta plain (Li et al., 2002; Hori et al., 2001) and the decline in the Yangtze sediment supply owing to weakening of the East Asian Summer Monsoon ~6000 years ago (Zhan et al., 2012). Rapid shoreline accretion only occurred over past 2000 years, in concert with an increase in sediment supply from human activity (Hori et al., 2001; Wang et al., 2011). Sediment cores from the south coastal plain of Hangzhou Bay demonstrate that rapid infilling of Hangzhou Bay occurred during the early Holocene (Gao and Collins, 2014; Zhang et al., 2015). A long period of sedimentary hiatus then occurred during the middle to late Holocene with return to net sedimentation in Hangzhou Bay only in the past 2000 years (Gao and Collins, 2014; Zhang et al., 2015).

Tide dominates the south Yangtze coast with a mean tidal range of 2.7 m (Chen et al., 1985). The Yaojiang Plain of south east Hangzhou Bay has a smaller mean tidal range of 1.85 m. Uehara et al. (2002) reconstructed the palaeotidal fields in the Yangtze Estuary and the east China marginal sea by including the effect of palaeo-topographic change from sedimentation since the Last Glacial Maximum. The simulated amplitude M_2 tide, which is the most significant component of tide in this region, was 1.0–1.2 m on the coast south to the Hangzhou Bay (including the Yaojiang Plain) and 1.2–1.4 m on the coast of Taihu Plain during the middle Holocene (6 ka; Uehara et al., 2002). It has increased to 1.2–1.6 m in the inner and south part of the Hangzhou Bay at the present day, while remaining at 1.0–1.2 m in the south east part of the Bay. Ground elevation is 0–2 m above present mean sea level (the Yellow Sea datum, MSL_{YSD}) in most of central Taihu Plain and Yaojiang Plain, and 2–5 m in the plains along Hangzhou Bay (Fig. 1B).

The Yushan site is located in the north east of Yaojiang Plain, between the edge of the upland and the floodplain (Fig. 1). The site was excavated by the Ningbo Municipal Institute of Cultural Relics and Archaeology over an area of 4300 m^2 during September, 2014 to January, 2015. Each excavation unit is 10 m × 10 m in size (Fig. 2A). The archaeological sequence spans from the early/middle Hemudu culture to the Song dynasty, with ten layers numbered top to bottom correlating to distinct lithology, sedimentology and archaeological finds across the site (Table 1). Individual cultural layers are typically 25–50 cm thick, with the whole sequence spanning 1–2.5

m across the site (Fig. 2B, C). The cultural layers onlap the weathered bedrock or hardened mud surfaces in excavation units close to the upland, such as T0410 and T0513. The Holocene base then dips rapidly and is buried below the floodplain (Fig. 2).

Among the 10 layers (Table 1), layers 9, 7, 6 and 3 are composed of organic-rich mud or peat that contain artefacts of prehistoric early and middle Hemudu, late Hemudu and Liangzhu cultures and from the Shang and Zhou dynasty, respectively. Layers 10, 8, 5 and 4 are devoid of any cultural artefacts and are considered to be formed without human disturbance. Note that layer 7 only occurs at the edge of the upland, such as in unit T0410 (Fig. 2C). In addition, an erosional surface is prominent on top of the peat layer 6a in many units, and this peat layer is totally eroded away even in those units close to the upland (Figs 2, 3). Together with the erosional surface, a sand ridge of 20–30 cm high and ca. 60 cm wide that was defined as layer 5b, dips from the edge of upland eastward and cuts into layer 6 (Fig. 3D–F). Gravels, fragments of Liangzhu artefacts and abundant plant fragments were present in the sand ridge. Mixtures of sand and mud, also defined as layer 5b, only occurs above the erosional surface in the area between the sand ridge and the upland.

3. Materials and Methods

During our excavation, we carefully examined the lithological and stratigraphic sequences in each excavation unit. We selected the north wall of unit T0415 for analyses of proxies including organic chemistry, diatoms and dinoflagellate cysts, because this unit is on the east edge of the excavation area where less human disturbance occurred (Fig. 2A). We also collected samples for these proxy analyses from unit T0410 because layer 7 is missing in unit T0415. We then identified the sedimentary facies of each layer and recognized marine inundation by examining the lithology and analysing proxies.

Twenty-seven (27) samples were collected from the north wall of unit T0415 for analyses of organic carbon and diatoms. Thirty-four (34) samples from layer 3 to 9 from the west wall of unit T0410 and seven samples from layer 6 of unit T0415 were collected for dinoflagellate cyst identification. In addition, seven tree stumps collected from the top of peat layer 6 in units T0214, T0314, T0315 and T0415 were identified at species level at the Institute of Archaeology, Chinese Academy of Social Science.

Samples for organic carbon measurement were dried at 40˚C in an oven and milled to powder. Two aliquots were prepared for each sample: (1) 20 mg powder was used to measure total carbon and total nitrogen (TN) using a vario MAX cube CN analyser (Elementar, Germany) (error <1%) at the State Key Laboratory of Marine Geology, Tongji University, China; (2) about 0.5 g powder was mixed with 0.1 M hydrochloric acid (HCl) for 24 hours to remove carbonate and then washed with deionized water thoroughly until the pH was neutral. The neutral specimen was dried at 40˚C and then used for measurement of TOC by vario MAX cube CN analyser (error <1%) at Tongji University and $\delta^{13}C_{V\text{-}PDB}$‰ (error, ±0.2‰; reference material: Urea and Acetanilide) by Delta V Advantage Isotope Ratio Mass Spectrometer

(Thermo Scientific, Germany) at the Third Institute of Oceanography, State Oceanic Administration of China. Samples for diatom analysis were prepared at Loughborough University in a water bath using 30% H_2O_2 to remove organic matter and HCl to remove carbonates, following the procedure of Renberg (1990), and permanent slides counted on a Leica DME light microscope (numerical aperture = 1.4) under oil immersion and phase contrast at x1000 magnification. Samples for dinoflagellate cysts identification were treated following standard procedures of pollen analysis (Moore et al., 1990) and the species were counted using a Leica optical microscope at x400 magnification. The identification of dinoflagellate cysts was made according to regional taxonomic guides (He et al., 2009; Mao et al., 2011; Tang et al., 2013).

For building the chronology, eight samples of charcoal, plant fragment and organic sediment from units T0410 and T0513 were AMS ^{14}C dated by Beta Analytic, USA, and calibrated using the Calib 7.1 program (Stuiver et al., 2015; Table 2). Furthermore, a sample from the sand ridge above the peat layer in T0513 (Fig. 3E) was dated using single-grain optically stimulated luminescence (OSL) measurement of quartz (Duller, 2008). In total, 3500 grains of quartz (180−224 µm) were measured and 37 grains were accepted for age determination (Table 3; Fig. S1). Luminescence measurements were carried out by an automated Risø-TL/OSL DA-20 DASH reader equipped with a $^{90}Sr/^{90}Y$ beta source (Bøtter-Jensen et al., 2003) and an ET EMD-9107 photomultiplier tube at the State Key Laboratory of Estuarine and Coastal Research, East China Normal University.

We also decided to use the south excavation wall of unit T0513 and west wall of unit T0410 for relative sea level reconstruction. In the south wall of unit T0513, the Holocene base of hardened mud dips gradually from west to east while peaty mud layer 9 and peat layer 6a formed the basal peat from east to west, respectively (Fig. 2B). In the west wall of unit T0410, as the thick layer of peat (layer 6) was eroded away and the sedimentary sequence above the Holocene base is only ~150 cm thick in the north part (Fig. 2C), sediment compaction can be neglected when applying the sea-level indicators from this profile. When collecting the radiocarbon dating material, three sample from layers 9, 8 and 6 in unit T0513, and three samples from layers 7, 4 and 3 in unit T0410 were chosen for reconstruction of relative sea levels (Fig. 2B, C; Table 4). We used the basal peat and stratigraphic approach to determine the palaeo-relative sea levels after identification of these sea-level indicators (Wang et al., 2013; Shennan et al., 2015). We used a total station to measure the elevation of the Holocene base in units T0410 and T0513, where samples of sea-level indicators were collected. We further used the tidal levels calculated from the records of Zhenhai gauge station (Fig. 1B) during AD 1958–1980 because a previous study simulated little change in the tidal range for the coast of Yaojiang Plain from the middle Holocene (6 ka) to the present day (Uehara et al., 2002). As a present-day, high-resolution topographic dataset (http://www.gscloud.cn) demonstrates that the present-day freshwater marsh mostly develops at ~0–0.5 m above the mean spring high water (MSHW) in the Yaojiang plain, freshwater marsh habitat inferred from palaeodata was therefore considered to be 0–0.5 m above the MSHW (Table 4).

In addition, we collected and recalibrated 80 published radiocarbon ages (Table S1) during and after the Liangzhu culture from Neolithic sites across the East China coastal plain using the Calib 7.1 programme (Stuiver et al., 2015) to revise the time span of the Liangzhu culture. We also compiled all published sedimentary profiles dated by AMS ^{14}C in the study area (Fig. S2 for their location) and compared the database covering the end of the Liangzhu culture which included radiocarbon ages (also recalibrated; Table S2), ecological and environmental proxies, and signals of flooding (Table 5).

4. Results

4.1 Holocene stratigraphy and sedimentary environmental change at Yushan

There is clear variation in organic geochemistry in each layer, distinguishing the terrestrial or marine source of organic carbon (Fig. 4). Diatom preservation is poor throughout much of the sequence, and identifiable valves were only observed in layers 9, 8 and 6, and in a single sample of layer 5. Such preservation problems are typical for coastal sediments (Ryves et al., 2004). By contrast, dinoflagellate cysts of marine genera including *Spiniferites*, *Operculodinium* and *Lingulodinium* were found in the non-cultural layers of 8, 5 and 4 and the bottom section of layer 3. Below we present the results of chronology, stratigraphic patterns of proxies and interpretation of sedimentary environments of layers 10–2.

Layer 10 (mud before the early Hemudu culture). Levels of TOC and TN are generally low (<1% and <0.2%, respectively; Fig. 4A) and values of TOC/TN and

$\delta^{13}C$ indicate that the dominant source of organic carbon was freshwater algae or freshwater particulate organic carbon (POC) (Fig. 4B; Lamb et al., 2006). A terrigenous environment is thus inferred for the Yushan site before the settlement of Hemudu people.

Layer 9 (early to middle Hemudu culture). A charcoal sample from this peaty mud layer was dated to 4440–4540 BCE (median age 4490 BCE; Table 2), which is in agreement with the artefacts of early to middle Hemudu culture found in this layer. TOC increases to ~5%; $\delta^{13}C$ analyses indicate that the organic carbon was derived from terrestrial C_3 plants and freshwater POC or algae (Fig. 4A, B). Diatoms are sparse in the bottom samples of this layer, consisting of robust, freshwater benthic forms. The middle sample in this section contained several whole cells of *Amphora copulata,* a benthic species more typical of higher conductivity freshwaters. The presence of whole cells suggests that the diatoms were growing *in situ*, rather than transported to the site, implying shallow water. Subsequent samples at the top of this layer 9 included taxa typical of somewhat fresher, low nutrient and lower pH waters, such as *Eunotia* and *Pinnularia*, along with some elongate *Fragilaria*. No marine dinoflagellate cysts was observed. A coastal freshwater marsh environment was identified during the early to middle Hemudu period.

Layer 8 (artefact-absent mud covering the early to mid-Hemudu cultural layer). A radiocarbon age of 4310 BCE (4260–4360 BCE) was obtained from a sample of plant fragments in the bottom section of this layer. TOC decreases sharply (<1%) and its isotopic composition demonstrates a terrestrial origin (Fig. 4B). However, a few valves of marine coastal taxa (such as *Rhaphoneis*) were encountered (Fig. 4A). Furthermore, of the four samples analysed, the uppermost sample had no marine dinoflagellate cysts, while concentrations for the other three were 332, 78 and 365 cysts g^{-1} dry weight (dw). An upper tidal flat environment was thus inferred at the site after the end of the middle Hemudu culture.

Layer 7 (late Hemudu culture). Radiocarbon dating of charcoal from this organic-rich mud layer gives an age of 4020 BCE (3945–4170 BCE; Table 2), supporting the finds of artefacts of late Hemudu culture found in this layer. Organic carbon was derived from freshwater algae or POC and some terrestrial C_3 plants (Fig. 4B). Only two samples contained marine dinoflagellate cysts among five samples in layer 7, with concentrations of 53 and 582 cysts g^{-1} dw. These data indicate a saltmarsh environment during the late Hemudu culture.

Layer 6 (Liangzhu culture). Radiocarbon ages from two samples from the bottom and upper section of this layer are 3570 BCE (3515–3640 BCE) and 2760 BCE (2635–2880 BCE), respectively (Table 2; Fig. 3A), which is consistent with the Liangzhu artefacts found in this layer. Rooted *in situ* at the top of this peat layer are many tree stumps at the edge of the excavation area (Fig. 3B, C), all of which have been identified as mature willow (*Salix*; ~12–25 cm in diameter; 1–6 trees per excavation unit of 100 m^2). This shrub is typical of the natural Yangtze coastal freshwater marsh, a zone located above MSHW (Zong et al., 2007; 2011). Both TOC and TN increase steadily throughout layer 6, reaching values of almost 21% (TOC) and 1% (TN). Values of $\delta^{13}C$ of approximately –28‰ and TOC/TN >15 imply that this OC was dominantly derived from terrestrial C_3 plants. Furthermore, a diverse flora of diatoms typical of shallow, freshwater/slightly brackish conditions appeared, including species of *Cymbella*, *Amphora*, *Gyrosigma*, *Nitzschia* and *Navicula*. Higher up the sequence, taxa typical of more distinctly brackish conditions were also found, including *Ctenophora pulchella*, *Rhopalodia gibba* and *Chaetoceros* cysts, as well as more clearly freshwater and low alkalinity taxa (*Eunotia*, *Pinnularia*, *Cocconeis*), suggesting a mixture of shallow wetland, freshwater and coastal marine habitats in the vicinity of the site. No marine dinoflagellate cysts was found. A coastal freshwater marsh close to the MSHW is inferred during the Liangzhu culture.

Layer 5b (gravelly sand, sand or sand-mud mixture cutting into the Liangzhu peat). The sedimentary composition of the sand ridge consisting of gravel, sand and fragments of the Liangzhu artefacts indicates strong hydrodynamic force during its formation. A radiocarbon age of 2760 BCE was derived from the plant fragments within the sand ridge, being identical with that of the underlying peat (Table 2), reflecting reworking from the peat. This sand ridge cutting into the peat layer, together with the sedimentary architecture including the erosional surface and tree stumps at the top of the underlying peat layer, reflect strong erosion and sudden deposition during a major storm event. Previous studies has reported similar deposition facies and sequences during storm events, such as the development of chenier ridges on the tidal flat of the Yangtze coast (Yan et al., 1989). OSL dating of single quartz grains within the sand ridge yielded an age of 4.59±0.24 ka BP (with a central age of 2575 BCE; Table 3).

Layer 5a (artefact-absent mud covering the Liangzhu layer). Similar to layer 8 which overlies the early to mid-Hemudu peat, layer 5a of homogenous mud overlays the Liangzhu peat in many units. At the bottom of this layer, TOC also abruptly declines to <1% similar to the change from layer 9 to layer 8, with a simultaneous dramatic increase in $\delta^{13}C$ (to –20.66‰) and a decrease in TOC/TN to <8 (Fig. 4A), implying that this organic matter was derived from marine algae or marine POC (Fig. 4B). In the upper part of layer 5, TOC increases slightly and $\delta^{13}C$ shifts to the freshwater algal or POC range, indicating a short period of desalinisation. Some valve fragments of marine plankton (such as large *Coscinodiscus*) were encountered in one sample. Concentration of marine dinoflagellate cysts were abundant (~700–1500 g^{-1} dw) in the whole section. Coastal marine sediment is thus inferred for this layer. We argue that this layer also represents the deposits of the storm event, due to its very high sedimentation rate compared to other layers, and the desalinisation signal inferred from the organic carbon source in the upper part (Fig. 4A). We suggest this mud layer was formed by rapid settling of suspended sediments after the storm, which reworked fine-grained sediments from offshore areas and transported these onshore. The increase in terrestrial organic carbon input in the upper section is an indication of the large amount input of freshwater discharge caused by intense precipitation associated with the storm.

Layer 4 (artefact-absent mud). An age of 2335–2495 BCE was derived from the bottom of this layer. TOC drops further and was dominated by marine POC or bacterial OC (Fig. 4). Some unidentifiable girdle bands of a large centric diatom, probably a marine planktonic species, was found in one sample. Concentration of marine dinoflagellate cysts is high (500–1500 g^{-1} dw). Together with the lithological feature of silt lamination, we suggest an upper tidal-flat environment during the formation period of layer 4.

Layers 3 (Shang to Zhou dynasty) and 2 (Tang to Song dynasty). The radiocarbon age of charcoal is 1395–1500 BCE at the bottom of this section, which together with artefacts of Shang to Song dynasties, provides firm evidence that these two layers were formed during the historical period. TOC/TN increased in layers 3 and 2, and OC is dominated by freshwater algae and the POC contains a signal of terrestrial C_3 plants (Fig. 4B). There are some marine dinoflagellate cysts (476 cysts g^{-1} dw) in the base of layer 3, indicating a saltmarsh environment at the beginning of Shang dynasty and a freshwater environment thereafter.

From the results of these multiproxy analyses of organic carbon sources, marine microfossils and the occurrence of human cultural layers, we speculate that humans settled at the Yushan site during periods when coastal freshwater marsh or saltmarsh environment prevailed over the last ~6500 years. However, such settlement was interrupted by two marine intrusion events, corresponding to the interruption of the Hemudu and termination of the Liangzhu culture during ~4310–4020 BCE and 2575–1450 BCE, respectively. Note that the later event was characterized by a major storm event at its beginning, a storm that was strong enough to erode away the peat layer and form a sand ridge.

4.2 Ages of the storm event and the terminal of Liangzhu culture

The OSL dating of quartz grains gives a direct age of 2575 ± 240 BCE for the sand ridge. However, a narrower age span is necessary to discuss the linkage between coastal flooding and the Neolithic culture. As the top of the peat unit at Yushan was eroded away by the storm in many units (Figs. 2, 3) or possibly lost due to human land use such as building an artificial platform (Table 1), we are unable to determine directly the age when the coastal marsh was inundated and buried by the marine sediments. We therefore compared the ages obtained from the rice field profiles at the Tianluoshan (TLS) site, which is only ~20 km away from Yushan and is located inland and surrounded by highland (Fig. 1B). At the TLS site, the top of the corresponding peat bed formed during the Liangzhu period is non-erosively preserved and dateable (Zheng et al., 2012). This implies that this site was protected from the storm erosion and only drowned by the sea water. Thus, the buried peat top should represent the original depositional surface of the coastal marsh. Two samples of seeds from different trenches from the peat top of the TLS site resulted in the same age of 2540 BCE (^{14}C ages of 4015 ± 45 and 4020 ± 40 yr BP, respectively, Table 2). This corresponds very well with the Yushan profile, both in terms of the stratigraphy and the age of the marine inundation as dated by OSL (2575 BCE; Table 3). From these two reliable and independent lines of chronological evidence which give a range of 2540–2575 BCE for the central age, we therefore consider that the most likely date of the storm to be ~2560 ± 100 BCE (the range of ± 100 years was decided according to the error of radiocarbon dating).

The Liangzhu people abandoned the Yushan site immediately after the storm event. Our compilation of radiocarbon ages of other sites across the south Yangtze coastal plains further demonstrates that the terminal age of the Liangzhu culture was at approximately 2500 BCE (Fig. 5), when the Liangzhu people abandoned their state capital complex (Zhang et al., 2015; Wang et al., 2017). Thus, the Liangzhu culture ended only decades after the Yushan storm. The subsequent Qianshanyang and Guangfulin cultures both lasted only for ~300 years, much shorter than the Liangzhu culture (Fig. 5).

4.3 Relative sea-level change from 4500 to 1500 BCE

The deposits of saltmarsh and freshwater marsh of layers 7 and 6, respectively imply that relative sea level dropped from −0.78 ± 0.22 m to −1.10 ± 0.25 m during the period from late Hemudu (3945–4170 BCE) to Liangzhu culture (2635–2880 BCE; Table 4; Fig. 6). We further interpolated an indicator of the peat top from the west part of unit T0513, where weak erosion of the peat occurred, and ~30-cm thick peat exists above the Holocene base (Fig. 2B). An original ~40-cm thickness of the peat was estimated using the highest estimation of percentage (30%) of peat compaction with an overburden of 1 m (van Asselen et al., 2011). Thus, the original altitude of the peat top and the relative sea level was estimated to be at 1.16 m and −0.70 ± 0.25 m, respectively (Table 4) when the storm occurred at 2560 ± 100 BCE. The upper tidal flat facies of layer 4 indicates a high relative sea-level stand at ~0.25 ± 0.27 m at 2335–2495 BCE while the saltmarsh sediments of layer 3 indicate the sea level was at ~0.05 ± 0.22 m at 1395–1500 BCE. These data suggest an acceleration in relative sea-level rise during the late stage of Liangzhu culture and a slight drop of the sea level from ~2440 BCE. In addition, a rapid relative sea-level rise also occurred from −1.49 ± 0.25 m to −0.45 ± 0.27 m from 4440–4540 BCE to 4260–4360 BCE, inferred from the basal peat layer 9 and the marine-originated homogenous mud layer 8, respectively (Figs 2B, 4; Table 4). Similarly, this earlier acceleration of sea-level rise occurred during the cultural interruption period between early to mid-Hemudu and late Hemudu cultures (Fig. 6).

5. Discussion

5.1 Flooding signatures across the south Yangtze coast

From these multiproxy and independent lines of evidence, we speculate that a major coastal storm occurred at ~2560 ± 100 BCE, which not only overwhelmed the Yushan site directly, but was strong enough to erode away ~30-cm thick peat (Fig. 3). This storm was followed by long-lasting marine inundation and the development of a brackish tidal flat owing to relative sea-level rise, which led to human abandonment of the area for ~1000 years until ~1625 BCE (Figs. 4, 6). The brackish wetland ecosystem was characterised by low primary productivity, bacterial-dominated OC and low terrestrial OC input, probably with limited biomass production, and was unlikely to support significant human populations during the high sea-level stand of 2440–1625 BCE (Fig. 4). Although the wetland had become less saline by the time of the subsequent Shang, Zhou, Tang and Song dynasties (layers 2 and 3), we infer from the geochemical data (especially TOC% and TOC/TN) that primary productivity was far lower than it had been during the Liangzhu period (Fig. 4A).

Comparisons with the data available from previous studies of the south Yangtze coast (Fig. 6; Table 5) reveal the extent of this coastal flooding in response to the accelerated sea-level rise during the later stages of Neolithic culture. As expected, a strong saline event occurred at ~2540 BCE at sites within the Yaojiang plain (cf. at TSL; Zheng et al., 2012), but it is also clearly seen 140 km west (at KHQ; ZPICRA, 2004; Fig. 6). A slight increase in salinity (reflected by increase in the abundance of saline Chenopodiaceae) was also seen at the Liangzhu site close to the state capital (Table 5). The marine flooding likely did not extend across the Taihu Plain, which also had some protection from substantial chenier ridges to the east (Fig. 1), but there is evidence of a salinization event at the same time at sites ZX-1, TMC (Fig. 6) and Guangfulin (Table 5) close to the shoreline. At most other sites, an increase in local water level was reported at the end of the Liangzhu period (Table 5), implying inland flooding from storm rainfall or waterlogging due to sea-level rise.

5.2 Causes of the mid-Holocene coastal flooding

Our reconstruction of relative sea level demonstrated a rapid rise (~0.95 m in ~120 years; Table 4) at the final stage of the Liangzhu culture (Fig. 6). The amplitude of this rise could be slightly overestimated because of the uncertainty in the height of the top of the peat and the underestimation of its compaction. We also did not consider the enlargement of the tidal range because previous simulations demonstrated little change in the amplitude of the M_2 tide in the south east Hangzhou Bay during the middle to late Holocene (Uehara et al., 2002). As previous studies further suggest no major deposition or shoreline advance during the middle Holocene along the Hangzhou Bay (Yan et al., 1989; Gao and Collins, 2014; Zhang et al., 2015), we infer no significant change in tidal levels after the Yushan storm ~4500 years ago.

This accelerated relative sea-level rise is consistent with sea level records from other regions around the world, and adds to evidence that this rise may reflect a global signal, rather than resulting from local processes. For example, on the coast of Peninsular Malaysia, the relative sea level dropped slightly from 3500 to 2500 BCE and then rose suddenly by ~1–3 m from ~2500 to 2100 BCE (Tjia, 1996; Horton et al., 2005). Rapid relative sea level rise between 2650 and 2350 BCE was also reported from the coast of north-eastern Brazil (~1 m; Suguio et al., 2013) and the northern Gulf of Mexico (Balsillie and Donoghue, 2011). In the mid-Pacific Ocean, microatolls record a relative sea level rise beginning at ~2500 BCE, following slightly declining or stable levels over the previous ~1500 years (Woodroffe et al., 2012). The eustatic sea level curve reconstructed from Red Sea corals shows that sea level began to rise at ~2300 BCE, following stable or declining levels over the previous ~900 years (Siddall et al., 2003). These data imply a small but significant acceleration in global sea level rise in the middle of the third millennium BCE.

In addition, Meltzner et al. (2017) reported a half-meter sea level excursion on centennial timescales between 6850 and 6500 cal yr BP from the microatolls of the Sunda Shelf, which indicates that the regional relative sea-level change could be a highly fluctuating pattern along the west coast of the Pacific Ocean. We infer that the rapid rise of relative sea level at Yushan ~4500 years ago, together with the earlier rise ~6300 years ago (Fig. 6) have similarity with the records in the microatolls of the Sunda Shelf. Furthermore, the record of the Asian summer monsoon shows a small peak in activity from ~2600–2450 BCE (Fig. 6; Wang et al., 2005). A comparison of values between the Dongge Cave $\delta^{18}O$, a proxy for the relative strength of the Asian summer monsoon, and atmospheric $\Delta^{14}C$, a proxy for solar activity, revealed that the monsoon peak coincided with the peak in solar irradiance from ~2600 to 2400 BCE (Stuiver, 1998; Wang et al., 2005). From these data, we infer that this small monsoon intensity peak was driven by increasing solar activity and hence was a climate-warming event on a centennial timescale. Therefore, we suggest that accelerated global sea-level rise occurred against a backdrop of climate warming during the late stage of the Liangzhu culture.

Previous studies suggested that a key feature of accelerated rising sea level is that the return periods of flood events decrease as the sea level increases (Sweet et al., 2014; Tessler et al., 2015). We thus suggest that the catastrophic storm at Yushan marked the beginning of a period of frequent flooding across the Yangtze coast, likely including other major coastal and inland flooding events, as supported by evidence of flood deposits in the coastal lowland of Hangzhou Bay and increasing freshwater levels across the Taihu Plain (Fig. 6; Table 5).

5.3 Impacts of the coastal flooding on the Liangzhu human society

We argue that perhaps only over a few decades, the combined effect of a series of extreme events and flooding, such as the Yushan inundation, could have overwhelmed even a politically advanced, technologically capable and well-organised prehistoric society such as the Liangzhu. Frequent extreme events and flooding would have had profound impacts, both immediate and longer-term. The coastal storm recorded at Yushan at 2560 BCE and associated flooding (including inland river flooding from storm rainfall) would have destroyed settlements and infrastructure across the region, as seen in the archaeological record at Yushan (Fig. 3). In the Yaojiang Plain, the immediate aftermath of marine flooding would have killed freshwater wetland plant communities that could not tolerate higher salinity and thus ended rice cultivation (Zheng et al., 2012); low net biomass production under marine/brackish conditions (Fig. 4A) would be unlikely to support significant human populations. At the head of Hangzhou Bay, coastal flooding also inundated the late-Liangzhu rice paddies such as at Maoshan (~30 km away from the Mojiaoshan, Fig. 1), notwithstanding it was designed with artificial ditches to facilitate water management (Zhuang et al., 2014). The political centre of Mojiaoshan was not only threatened directly by the salt intrusion and frequent flooding (Liu and Chen, 2012;

Zhuang et al., 2014; Table 4), but also could have learned lessons from the flooding of inundated sites in the Yaojiang Plain.

Furthermore, although societal and demographic recovery from a single extreme event could have happened after the Yushan storm (e.g. during freshening seen in the upper section of layer 5; Fig. 4A), frequent flooding would have made this much more difficult, for example by ruining stored rice seeds or from persistent and widespread crop failure (Stone, 2009). This would quickly result in a shortage of surplus production needed to support the political centre, and the large number of artisanal workers not employed in food production, such as jade workers (Liu and Chen, 2012). It is possible that the Liangzhu ruling political elite could have moved the state capital away from the coastal lowland as an adaptive strategy to mitigate the impacts of rising sea level and increasing flooding, potentially explaining the appearance of the subsequent, but less organised and less developed (yet culturally related), Qianshanyang culture. Owing to its profound impacts on the landscape and people, this period of flooding, including the Yushan storm at 2560 BCE, may even have contributed to the ancient oral flood traditions in the Lower Yangtze, forming the cultural setting for the legend of China's Great Flood more than 4000 years ago (Lewis, 2006).

6. Conclusions

From the sedimentary record at the Yushan archaeological site, and combined evidence from other sites in the south Yangtze coastal plain, we conclude that major coastal flooding occurred at the late stage of the Liangzhu culture. This flooding was characterized by extreme events, and was caused by short-term but significant acceleration in sea-level rise, which was possibly linked to a climate warming event on a centennial timescale. We suggest that the frequent extreme events and catastrophic flooding during warming climate phases are controlling factors in explaining Neolithic cultural transitions in the middle Holocene in the Yangtze coastal lowland, including the sudden and perplexing demise of the technologically advanced Liangzhu culture. Our finding of this catastrophic coastal flooding at the middle of third millennium BCE provides an analogue for flood risk, owing to the predicted high rate of sea level rise at the end of 21st century (Nerem et al., 2018) and urgently calls for mitigation strategies to be put in place to protect vulnerable coastal populations worldwide against a similar scenario of abrupt sea level rise in the near future.

Acknowledgements

This study was supported by the National Natural Science Foundation of China (Grant No. 41576042). We are grateful to two anonymous reviewers for their helpful comments.

References

Atahan, P., Itzstein-Davey, F., Taylor, D., Dodson, J., Qin, J., Zheng, H., Brooks, A., 2008. Holocene-aged sedimentary records of environmental changes and early agriculture in the lower Yangtze, China. Quaternary Science Reviews 27, 556−570, doi:10.1016/j.quascirev.2007.11.003.

Balsillie, J.H., Donoghue, J.F., 2011. Northern Gulf of Mexico sea-level history for the past 20,000 years. In: Buster, N.A., and Holmes, C.W., eds, Gulf of Mexico Origin, Waters, and Biota: Volume 3, Geology. Texas A&M University Press, Texas, pp 53–72.

Bøtter-Jensen, L., Andersen, C.E., Duller, G.A.T., and Murray, A.S., 2003. Developments in radiation, stimulation and observation facilities in luminescence measurements. Radiation Measurements 37, 535–541, doi: 10.1016/S1350-4487(03)00020-9.

Chen, J., 2002. The Neolithic culture and environment in the Yangtze delta plain. PhD. Thesis, Shanghai, East China Normal University, 109 p (in Chinese).

Chen, J.Y., Zhu, H.F., Dong, Y.F., Sun, J.M., 1985. Development of the Changjiang estuary and its submerged delta. Continental Shelf Research 4, 47–56.

Chen, Z., Wang, Z., Schneiderman, J., Cai, Y., 2005. Holocene climate fluctuations on millennium scale in the Yangtze delta of eastern China: implications and response. The Holocene 15, 917–926.

Duller, G.A.T., 2008. Single-grain optical dating of Quaternary sediments: why aliquot size matters in luminescence dating. Boreas 37, 589–612, doi: 10.1111/j.1502-3885.2008.00051.x.

Durcan, J.A., King, G.E., Duller, G.A.T., 2015. DRAC: Dose rate and age calculation for trapped charge dating. Quaternary Geochronology 28, 54−61.

Gao, S., Collins, M.B., 2014. Holocene sedimentary systems on continental shelves. Marine Geology 352, 268–294.

Giosan, L., Syvitski, J., Constantinescu, S., Day, J., 2014. Climate change: protect the world's deltas. Nature 516, 31–33.

He, C.Q., Song, Z.C., Zhu, Y.H., 2009. Dinoflagellate fossil of China. Science Press, Beijing (in Chinese).

Hori, K., Saito, Y., Zhao, Q., Cheng, X., Wang, P., Sato, Y., Li, C., 2001. Sedimentary facies of the tide-dominated paleo-Changjiang (Yangtze) estuary during the last transgression. Marine Geology 177, 331–351.

Horton, B.P., Gibbard, P.L., Milne, G.M., Morley, R.J., Purintavaragul, C., Stargardt, J.M., 2005. Holocene sea levels and palaeoenvironments, Malay-Thai Peninsula, southeast Asia. The Holocene 15, 1199–1213.

Innes, J.B., Zong, Y., Wang, Z., and Chen, Z., 2014. Climatic and palaeoecological changes during the mid- to Late Holocene transition in eastern China: high-resolution pollen and non-pollen palynomorph analysis at Pingwang, Yangtze coastal lowlands. Quaternary Science Reviews 99, 164–175, doi: 10.1016/j.quascirev.2014.06.013.

Itzstein-Davey, F., Atahan, P., Dodson, J., Taylor, D., Zheng, H., 2007. Environmental and cultural changes during the terminal Neolithic: Qingpu, Yangtze delta, eastern China. Holocene 17, 875−887, doi:10.1016/j.quascirev.2007.11.003.

Kopp, R.E., Kemp, A.C., Bittermann, K., Horton, B.P., Donnelly, J.P., Gehrels, W.R., Hay, C.C., Mitrovica, J.X., Morrow, E.D., and Rahmstorf, S., 2016. Temperature-driven global sea-level variability in the Common Era. Proc. Natl. Acad. Sci. USA 113, E1434–E1441, doi: 10.1073/pnas.1517056113.

Lamb, A.L., Wilson, G.P., and Leng, M.J., 2006. A review of coastal palaeoclimate and relative sea-level reconstructions using $\delta^{13}C$ and C/N ratios in organic material. Earth-Science Reviews 75, 29–57, doi: 10.1016/j.earscirev.2005.10.003.

Lawler, A., 2009. Beyond the Yellow River: how China became China. Science 325, 930–935, doi: 10.1126/science.325_930.

Lewis, M.E., 2006. The Flood Myths of Early China. New York, State University of New York Press, 256 p.

Li, C., Wang, P., Sun, H., Zhang, J., Fan, D., Deng, B., 2002. Late Quaternary incised-valley fill of the Yangtze delta (China): its stratigraphic framework and evolution. Sedimentary Geology 152, 133–158.

Li, Y., Wu, J., Hou, S., Shi, C., Mo, D., Liu, B., Zhou, L., 2010. Palaeoecological records of environmental change and cultural development from the Liangzhu and Qujialing archaeological sites in the middle and lower reaches of the Yangtze River. Quaternary International 227, 29−37, doi:10.1016/j.quaint.2010.05.015.

Liu, L., Chen, X., 2012. The Archaeology of China: From the Late Paleolithic to the Early Bronze Age (Cambridge World Archaeology). Cambridge, Cambridge University Press, 475 p.

Liu, C., Sui, J., He, Y., Hirshfield, F., 2013. Changes in runoff and sediment load from major Chinese rivers to the Pacific Ocean over the period 1955–2010. International Journal of Sediment Research 28, 486–495.

Liu, B., Wang, N., Chen, M., Wu, X., Mo, D., Liu, J., Xu, S., Zhuang, Y., 2017. Earliest hydraulic enterprise in China, 5,100 years ago. PNAS 114, 13637–13642.

Mao, L.M., Wang, W.M., Shu, J.W., Yang, X.L., 2011. Holocene spores and microscopic algae from the Yangtze delta, east China Acta palaeontologica Sinica 50, 154–165 (in Chinese, with English abstract).

Meltzner, A.J., Switzer, A.D., Horton, B.P., Ashe, E., Qiu, Q., Hill, D.F., Bradley, S.L., Kopp, R.E., Hill, E.M., Majewski, J.M., Natawidjaja, D.H., and Suwargadi, B.W., 2017. Half-metre sea-level fluctuations on centennial timescales from mid-Holocene corals of Southeast Asia. Nature Communications 8, 14387, doi: 10.1038/ncomms14387.

Moore, P.D., Webb, J.A., Collinson, M.E., 1990. Pollen analysis. Blackwell Scientific Publications, Oxford.

Nerem, R.S., Beckley, B.D., Fasullo, J.T., Hamlington, B.D., Masters, D., Mitchum, G.T., 2018. Climate-change-driven accelerated sea-level rise detected in the altimeter era. Proc. Natl. Acad. Sci. USA, doi: 10.1073/pnas.1717312115.

Nicholls, R.J., and Cazenave, A., 2010. Sea-level rise and its impact on coastal zones. Science 328, 1517–1520, doi: 10.1126/science.1185782.

Qin, L., 2013. The Liangzhu Culture. In: Underhill, A.P. (ed.), A Companion to Chinese Archaeology. Wiley-Blackwell, pp 574−598.

Qin, J., Taylor, D., Atahan, P., Zhang, X., Wu, G., Dodson, J., Zheng, H., Itzstein-Davey, F., 2011. Neolithic agriculture, freshwater resources and rapid environmental changes on the lower Yangtze, China. Quaternary Research 75, 55−65, doi: 10.1016/j.yqres.2010.07.014.

Renberg, I., 1990. A procedure for preparing large sets of diatom slides from sediment cores. Journal of Paleolimnology 4, 87–90.

Ryves, D.B., Clarke, A.L., Appleby, P.G., Amsinck, S.L., Jeppesen, E., Landkildehus, F., and Anderson, N.J., 2004. Reconstructing the salinity and environment of the Limfjord and Vejlerne Nature Reserve, Denmark, using a diatom model for brackish lakes and fjords. Canadian Journal of Fisheries & Aquatic Sciences 61, 1988–2006, doi: 10.1139/F04-127.

Shanghai Museum, 2002. The excavated report on the Neolithic site GUANG FU LIN, Songjiang, Shanghai during 1999-2000. KAO GU (10), 31−48 (in Chinese).

Shennan, I., Long, A.J., Horton, B.P., 2015. Handbook of sea-level research. John Wiley &Sons, Ltd.

Siddall, M., Rohling, E.J., Almogi-Labin, A., Hemleben, Ch., Meischner, D., Schmelzer, I., and Smeed, D.A., 2003. Sea-level fluctuations during the last glacial cycle. Nature 423, 853–858, doi: 10.1038/nature01690.

Stanley, D.J., Chen, Z., and Song, J., 1999. Inundation, sea-level rise and transition from Neolithic to Bronze age cultures, Yangtze delta, China. Geoarchaeology 14, 15–26.

Stone, R., 2009. One year after a devastating cyclone, a bitter harvest. Science 324, 715, doi: 10.1126/science.324_715.

Stuiver, M., 1998. INTCAL 98 radiocarbon age calibration, 24,000-0 cal BP. Radiocarbon 40, 1041–1083.

Stuiver, M., Reimer, P.J., Reimer, R., 2015. CALIB: Radiocarbon Calibration: http://calib.qub.ac.uk/calib/(September 2015).

Sun, D., Gagan, M.K., Cheng, H., Scott-Gagan, H., Dykoski, C.A., Edwards, R.L., and Su, R., 2005. Seasonal and interannual variability of the Mid-Holocene East

Asian monsoon in coral $\delta^{18}O$ records from the South China Sea. Earth and Planetary Science Letters 237, 69–84.

Suguio, K., Barreto, A.M.F., de Oliveira, P.E., Bezerra, F.H.R., and Vilela, M.C.S.H., 2013. Indicators of Holocene sea level changes along the coast of the states of Pernambuco and Paraíba, Brazil. Geologia USP 13, 141–152, doi: 10.5327/Z1519-874X201300040008.

Sweet, W., Park, J., Marra, J., Zervas, C., and Gill, S., 2014. Sea level rise and nuisance flood frequency changes around the United States. NOAA Technical Report NOS CO-OPS 073, 58 p.

Syvitski, J.P.M., Kettner, A.J., Overeem, I., Hutton, E.W.H., Hannon, M.T., Brakenridge, G.R., Day, J., Vorosmarty, C., Saito, Y., Giosan, L., and Nicholls, R.J., 2009. Sinking deltas due to human activities. Nature Geoscience 2, 681–686.

Tang, L.Y., Mao, L.M., Li, X.M., 2013. Palaeoecological and palaeoenvironmental significance of some important spores and micro-algae in Quaternary deposits. Chinese Science Bulletin 58, 3125–3139.

Tessler, Z.D., Vörösmarty, C.J., Grossberg, M., Gladkova, I., Aizenman, H., Syvitski, J.P.M., and Foufoula-Georgiou, E., 2015. Profiling risk and sustainability in coastal deltas of the world. Science 349, 638–643, doi: 10.1126/science.aab3574.

Tjia, H.D., 1996. Sea-level changes in the tectonically stable Malay-Thai Peninsular. Quaternary International 31, 95–101.

Uehara, K., Saito, Y., Hori, K., 2002. Paleotidal regime in the Changjiang (Yangtze) Estuary, the East China Sea, and the Yellow Sea at 6 ka and 10 ka estimated from a numerical model. Marine Geology 183, 179–192.

van Asselen, S., Karssenberg, D., Stouthamer, E., 2011. Contribution of peat compaction to relative sea-level rise within Holocene deltas. Geophysics Research Letters 38, L24401, doi:10.1029/2011GL049835.

Wang, X., Mo, D., Li, C., Yu, S.-Y., Xue, B., Liu, B., Wang, H., and Shi, C., 2017. Environmental changes and human activities at a fortified site of the Liangzhu culture in eastern China: evidence from pollen and charcoal records. Quaternary International 438, 189–197, doi: 10.1016/j.quaint.2017.05.001.

Wang, Y., Cheng, H., Edwards, R.L., He, Y., Kong, X., An, Z., Wu, J., Kelly, M.J., Dykoski, C.A., and Li, X., 2005. The Holocene Asian monsoon: links to solar changes and North Atlantic climate. Science 308, 854–857, doi: 10.1126/science.1106296.

Wang, Z., Li, M., Zhang, R., Zhuang, C., Liu, Y., Saito, Y., Xie, J., Zhao, B., 2011. Impacts of human activity on the late-Holocene development of the subaqueous Yangtze delta, China, as shown by magnetic properties and sediment accumulation rates. The Holocene 21, 393–407.

Wang, Z., Zhuang, C., Saito, Y., Chen, J., Zhan, Q., and Wang, X., 2012. Early mid-Holocene sea-level change and coastal environmental response on the southern Yangtze delta plain, China: implications for the rise of Neolithic culture. Quaternary Science Reviews 35, 51–62, doi: 10.1016/j.quascirev.2012.01.005.

Wang, Z., Zhan, Q., Long, H., Saito, Y., Gao, X., Wu, X., Li, L., Zhao, Y., 2013. Early to mid-Holocene rapid sea-level rise and coastal response on the southern Yangtze delta plain, China. Journal of Quaternary Science 28, 659–672.

Woodroffe, C.D., McGregor, H.V., Lambeck, K., Smithers, S.G., and Fink, D., 2012. Mid-Pacific microatolls record sea-level stability over the past 5000 yr. Geology 40, 951–954, doi: 10.1130/G33344.1.

Woodruff, J.D., Irish, J.L., and Camargo, S.J., 2013. Coastal flooding by tropical cyclones and sea-level rise. Nature 504, 44–52, doi: 10.1038/nature12855.

Yan, Q., Xu, S., and Shao, X., 1989. Holocene cheniers in the Yangtze Delta, China. Marine Geology 90, 337–343.

Zhan, Q., Wang, Z., Xie, Y., Xie, J., He, Z., 2011. Assessing C/N and $\delta^{13}C$ as indicators of Holocene sea level and freshwater discharge changes in the subaqueous Yangtze delta, China. The Holocene 22, 697–704.

Zhang, X., Dalrymple, R.W., Yang, S.-Y., Lin, C.-M., Wang, P., 2015. Provenance of Holocene sediments in the outer part of the paleo-Qiantang River estuary, China. Marine Geology 366, 1–15.

Zhang, X., Huang, D., Deng, H., Snape, C., Meredith, W., Zhao, Y., Du, Y., Chen, X., and Sun, Y., 2015. Radiocarbon dating of charcoal from the Bianjiashan site in Hangzhou: New evidence for the lower age limit of the Liangzhu Culture. Quaternary Geochronology 30, 9–17, doi: 10.1016/j.quageo.2015.07.001.

Zhao, X., 1998. Origin of rice paddy cultivation at the Hemudu site. Agricultural Archaeology 1, 131−137. Scanned by Sui, K.; form. by Leir, G.; transl./ed. by Gordon, B., Wong, E., Craig, A..

Zheng, Y., Sun, G., Qin, L., Li, C., Wu, X., and Chen, X., 2009. Rice fields and modes of rice cultivation between 5000 and 2500 BC in east China. Journal of Archaeological Science 36, 2609–2616, doi: 10.1016/j.jas.2009.09.026.

Zheng, Y.F., Sun, G.P., and Chen, X.G., 2012. Response of rice cultivation to fluctuating sea level during the Mid-Holocene. Chinese Science Bulletin 57, 370–378, doi: 10.1007/s11434-011-4786-3.

Zhuang, Y., Ding, P., and French, C., 2014. Water management and agricultural intensification of rice farming at the late-Neolithic site of Maoshan, Lower Yangtze River, China. The Holocene 24, 531–545, doi: 10.1177/0959683614522310.

Zong, Y., Chen, Z., Innes, J.B., Chen, C., Wang, Z., and Wang, H., 2007. Fire and flood management of coastal swamp enabled first rice paddy cultivation in east China. Nature 449, 459–462, doi: 10.1038/nature06135.

Zong, Y., Innes, J.B., Wang, Z., and Chen, Z., 2011. Mid-Holocene coastal hydrology and salinity changes in the east Taihu area of the lower Yangtze wetlands, China. Quaternary Research 76, 69–82, doi:10.1016/j.yqres.2011.03.005.

Zong, Y., Innes, J.B., Wang, Z., and Chen, Z., 2012. Environmental change and Neolithic settlement movement in the lower Yangtze wetlands of China. The Holocene 22, 659–673, doi: 10.1177/0959683611414933.

ZPICRA, 2004. KUA HU QIAO-Archaeological Report of Puyang River Valley I. Beijing, WEN WU Press, 379 p (in Chinese).

ZPICRA, Huzhou Museum, 2014. Qianshanyang: a report on the third and fourth excavations of the site. Beijing, WEN WU Press, 738 p (in Chinese).

Table headings

Table 1 A summary of the archaeological sequence at Yushan site (Figs 2, 3).

Table 2 AMS ^{14}C ages and their calibrations for the Yushan and Tianluoshan sites.

Table 3 Single-grain OSL age for the sand ridge sample from the Yushan site together with supporting dose rate and equivalent dose (D_e) data.

Table 4 Reconstruction of relative sea levels using sea-level indicators obtained from units T0410 and T0513 (Fig. 2B, C). Sedimentary facies was determined according to the lithology, organic carbon, diatom assemblage and dinoflagellate cysts. Tidal levels were collected from the Zhenhai gauge station (Fig. 1; 1958–1980). MSHW, 1.61 m; MHW, 1.17 m; MNHW, 0.63 m. All heights are given with respect to current mean sea level (Yellow Sea datum). Abbreviations: MSHW, mean spring high water; MHW, mean high water; MNHW, mean neap high water.

Table 5 Sediment profiles with high-resolution AMS ^{14}C ages from the Taihu and Yaojiang Plains and head of the Hangzhou Bay, East China coast. Locations of these profiles are indicated in Fig. S2.

Figure legends

Figure 1 Location maps. (**A**) East Asia and the location of the study area. (**B**) The south Yangtze coastal plain, showing the locations of the Liangzhu sites and all sites for which radiocarbon dates for the Liangzhu and post-Liangzhu cultural layers were available. These sites are numbered in sequence according to their distance from the Yushan site (Table S1). Note that the Liangzhu settlements are distributed mainly on the Taihu Plain of the southern Yangtze Delta plain and the Yaojiang Plain on the south east bank of Hangzhou Bay. (**C**) The flooding to a depth of >0.5 m across most of the Yaojiang Plain caused by Typhoon Fitow (the strongest typhoon to make landfall in China for over 60 years), October 2013 (data source: Ningbo gauge station, 2013. http://www.nbswz.com.cn/Html/201405/26/11669.html). (**D**–**F**) Typical artefacts of the Liangzhu culture discovered from the Yushan site, now deposited in Ningbo Municipal Institute of Cultural Relics and Archaeology. (**D**) Stone cutter (*Shi Dao*); (**E**) stone woodworking tool (*Youduan Shi Beng*); (**F**) black pottery two-lugged necked jar (*Shuangbi Hu*), with some remains of black slip. The maps were generated with the ArcGis 10.1 software (www.esrichina.com.cn) using the topographic dataset provided by the International Scientific & Technical Data Mirror Site, Computer Network Information Centre, Chinese Academy of Sciences (http://www.gscloud.cn).

Figure 2 (**A**). Aerial photo of the Yushan site during excavation. (**B**) Photo of the south wall of unit T0513. Numbers represent the cultural layers. Note layers 8 and 9 pinch out and disappear westward due to the basal topography, making layer 6 the Holocene basal peat in some sections. (**C**) Photo of the west wall of unit T0410. Numbers represent the cultural layers. The data set of altitude and radiocarbon age are presented for each sea-level indicator in (B) and (C). Layers 8 and 9 also pinch out and disappear northward due to the basal topography, making layer 7 the Holocene basal sediments. Elevation of the Holocene bases in two units were measured by a total station. White arrows with elevation and calibrated ages (BCE) represent data used for reconstruction of relative sea level. Numbers of cultural layers: **2**, Tang to Song dynasties; **3**, Shang to Zhou dynasties; **4**–**5**, natural deposits; **6a**–**6b**, Liangzhu period; **7**, late Hemudu period, missing in these units; **8**, natural deposits; **9**, early to middle Hemudu period; **10**, pre-Hemudu natural deposits.

Figure 3 Photographs of strata at Yushan. (**A**) Excavation unit T0513, showing the sediments deposited since the pre-Hemudu period and the erosional surface above the peat layer of the Liangzhu period. (**B**–**C**) Tree stumps on the tops of the peat layers in T0213 and T0214. (**D**) Sand ridge in T0415. (**E**–**F**) Sand ridge in T0513.

Figure 4 Environmental change and human responses at Yushan. (**A**) Stratigraphic patterns of total nitrogen (TN), total organic carbon (TOC), TOC/TN, bulk organic carbon stable isotopic composition ($\delta^{13}C$), dinoflagellate cysts, diatoms (N = none, F/B = freshwater/brackish; M = marine; detailed information in Table S4) and sedimentation rates (SR) in different cultural layers (2–10). The numbers used for the cultural layers are the same as in Fig. 3. Ages with stars (*) were calculated based on sedimentation rates. (**B**) Discrimination of organic carbon sources based on TOC/TN and $\delta^{13}C$ (adapted from Lamb et al., 2006).

Figure 5 Time span of the Liangzhu (Group 1), Qianshanyang (Group 2), Guangfulin (Group 3) cultures and post-Liangzhu natural deposits in Yaojiang plain (Group 4). Note the end of the Liangzhu culture is around 2500 BCE. Also indicated is the OSL age of the storm sand at the top of the Liangzhu cultural layer (boundary of layer 5/6a; Fig. 3). Site number ordered by distance from the Yushan site (Fig. 1; Table S1). Samples dated by AMS ^{14}C are indicated in red. Others were dated by the radiometric method.

Figure 6 Comparison of the relative sea-level change and regional marine flooding records on the south Yangtze coast from the Yaojiang and Taihu plains and the head of Hangzhou Bay. In the sea-level curve, calibrated radiocarbon ages are presented with error bars of 2σ; horizontal error bars represent the indicative meaning (range of relative sea level) of each sea-level indicator. The interpolated data point is calculated from the data set derived from the estimated storm age and original peat top (Table 4; see text for details). Sediment profiles are numbered as in Fig. S2 (with increasing distance from Yushan); data sources are given in Tables 4 and S2.

The oxygen isotopic record ($\delta^{18}O$) of stalagmite DA from Dongge Cave (the cave location is marked in Fig. 1A; Wang et al., 2005) denotes a short period of strengthening, yet variable, Asian summer monsoon linked to the warming climate (denoted by the red arrow) during the latter stages of the Liangzhu culture.

Table 1 A summary of the archaeological sequence at Yushan site (Figs 2, 3).

Cultural layer	Description of lithology	Archaeological finds	Cultural period
1	Cultivated layer.	None	Present-day
2	Yellowish earth.	Yue Kiln	Tang and Song
3	Dark grey or yellowish grey mud.	Pottery vessels, early proto-celadon, bronze ware, stone and wood tools	Shang and Zhou
4	Yellowish grey mud with some very thin (<1 mm) laminations of silt and abundant root traces.	None	Cultural interruption
5a	Grey homogeneous mud with an unconformity with the underlying layer 6.	None	Cultural interruption
5b	Gravelly sand, sand or mixture of sand and mud.	Some fragments of Liangzhu artefacts.	Storm deposits
6	a, peat; b, peaty mud. On top of this peat layer, an erosional surface occurred and tree stumps exist in many units (Fig. 3A–C).	An artificial platform occurred at the edge of upland, containing pottery vessels, polished stone tools of axe, adze, plow, cutter, arrowhead, sickle and *Mopan* slab. Some artefacts were also found in the peaty mud and peat.	Liangzhu

7	Organic rich mud	Red pottery vessels, polished stone tools of axe, adze, chisel, arrow head and *Mopan* slab and jade.	Late Hemudu
8	Grey homogeneous mud.	None	Cultural interruption
9	Dark grey peaty mud	Black pottery vessels, polished stone tools of axe and adze, bone awl and remains of architecture.	Early to middle Hemudu
10	Yellowish grey or grey homogeneous mud	None	Natural deposition before settling

Table 2 AMS ^{14}C ages and their calibrations for the Yushan and Tianluoshan sites.

Field number	Cultural period	Cultural layer (Fig. 3)	Dating material	$\delta^{13}C$ (‰)	Conventional age aBP	Calibrated age (BCE) 2 sigma	Probability	Median	Laboratory Number
T0410-3c	Shang	3	Charcoal	−25.2	3170 ± 30	1395–1500	1	1450	414776
T0410-4	None	4	Plant fragments	−27.9	3940 ± 30	2335–2495	0.90	2440	414777
T0513-5*	None	5	Plant fragments	−25.5	4170 ± 30	2635–2880	1	2760	406454
T0513-6a	Liangzhu	6a	Plant fragments	−30.3	4170 ± 30	2635–2880	1	2760	406455
T0410-6b	Liangzhu	6b	Organic sediments	−27.6	4770 ± 30	3515–3640	0.98	3570	414778
T0410-7	Late Hemudu	7a	Charcoal	−25.6	5210 ± 50	3945–4170	0.94	4020	414779
T0513-8-1	None	8	Plant fragments	NA	5470 ± 30	4260–4360	1	4310	406456
T0513-9	Early to mid-Hemudu	9	Charcoal	−26.3	5640 ± 30	4440–4540	0.83	4490	406457
Tianluoshan†	End of the Neolithic	–	Seeds	NA	4020 ± 40	2465–2635	0.98	2540	BA091045
Tianluoshan‡	End of the Neolithic	–	Seeds	NA	4015 ± 45	2455–2675	0.97	2540	BA07761

* This sample was collected from the sand ridge.

†, ‡ Ages for Tianluoshan were obtained from Zheng et al., (2009; 2012) and recalibrated using the Calib 7.1 program, as were other ages in the present study.

Table 3 Single-grain OSL age for the sand ridge sample from the Yushan site together with supporting dose rate and equivalent dose (D_e) data.

Lab No.	U (ppm)	Th (ppm)	K (%)	Water content (%)	Environmental dose rate[*] (Gy/ka)				Over-dispersion	D_e[†] (Gy)	Age ka	Calibrated calendar age (BCE)
					Beta	Gamma	Cosmic-ray	Total				
L144	3.5 ± 0.13	16.3 ± 0.39	2.01 ± 0.06	19 ± 5	1.77 ± 0.10	1.36 ± 0.07	0.18 ± 0.12	3.31 ± 0.12	0.18 ± 0.03	15.2 ± 0.57	4.59 ± 0.24	2575 ± 240[$]

[*] The dose rate and OSL ages were calculated using the 'DRAC' (Durcan et al., 2015).

[†] Single grains of quartz were measured in the regenerative-dose protocol, using a test-dose of 3.03 Gy, a preheat of 200 °C for 10 s, a 160 °C cut heat for 0 s, and green-laser stimulation at 125 °C for 0.9 s. The first 0.06 s of stimulation minus a background estimated from the integral of the last 0.1 s was used for single grain D_e calculation.

[$] This calibrated calendar age was calculated by subtracting 2015 that is the sampling year of the sand ridge from the OSL-dated age 4.59±0.24 ka.

Table 4 Reconstruction of relative sea levels using sea-level indicators obtains from units T0410 and T0513 (Fig. 2B, C). Sedimentary facies was determined according to the lithology, organic carbon, diatoms and dinoflagellate cysts. Tidal levels were collected from the Zhenhai gauge station (Fig. 1; 1958–1980). MSHW, 1.61 m; MHW, 1.17 m; MNHW, 0.63 m. All heights are given with respect to current mean sea level (Yellow Sea datum). Abbreviations: MSHW, mean spring high water; MHW, mean high water; MNHW, mean neap high water.

Unit	Alt. (m)	Cultural layer	Sedimentary facies	Calibrated age (BCE)	Indicative meaning	Palaeo-sea level (m)	Error (m)
T0410	1.44	3	Saltmarsh	1395–1500	MHW–MSHW	0.05	0.22
T0410	1.15	4	Upper tidal flat	2335–2495	MNHW–MHW	0.25	0.27
T0513	1.16†	6	Freshwater/ brackish marsh	2560*	0–0.5 m above MSHW	−0.70	0.25
T0513	0.76	6	Freshwater marsh	2635–2880	0–0.5 m above MSHW	−1.10	0.25
T0410	0.61	7	Saltmarsh	3945–4170	MHW–MSHW	−0.78	0.22
T0513	0.45	8	Upper tidal flat	4260–4360	MNHW–MHW	−0.45	0.27
T0513	0.37	9	Freshwater marsh	4440–4540	0–0.5 m above MSHW	−1.49	0.25

* This is the interpolated age, i.e., the age of storm event that drowned the peat layer.

† Calibrated value of the original peat top assuming that the peat layer above Holocene base in the west part of T0513 was ~30-cm thick, and had been compacted from an original ~40-cm thick layer, using the highest estimation of percentage (30%) of peat compaction with an overburden of 1 m (van Asselen et al., 2011).

Table 5 Sediment profiles with high-resolution AMS ^{14}C ages from the Taihu and Yaojiang Plains and head of the Hangzhou Bay, East China coast. Locations of these profiles are indicated in Fig. S2.

No. (Fig. 1)	Name of site	Dated period (BCE unless stated as AD)	Number of dates from 2000−3000 BCE	Covering the end of Liangzhu culture (Y/N)	Ecological and environmental indicators at the end of Liangzhu culture (Y/N)	Proxy	Signal of flooding	Data source
1	Yushan	1450-4490	4+1 (OSL)	Y	Y (sedimentation rate:0.5−4 mm yr^{-1})	Lithology, sedimentology, organic geochemistry, diatom, macroflora	Storm and marine flooding	Present study
2	Tianluoshan (TLS)	0-5080	2	Y	Y	Diatom, phytoliths, macroflora	Marine flooding	Zheng et al., 2016
3	Kuahuqiao (KHQ)	1160-9020	1	Y	Y	Lithology	Marine flooding	ZPICRA, 2004
4	Tangmiaocun (TMC)*	2730-4020	1	Y	Y	Diatom, rice phytoliths	Slight increase in salinity	Zong et al., 2011
5	ZX-1	685-6650	1	Y	Y	Pollen, foraminifera	Marine flooding	Stanley et al., 1999; Chen et al., 2005

6	Pingwang	860-5225	0	Y	Limited data due to very low sedimentation rate (0.1 mm yr^{-1})	Pollen	Increase in local water level	Innes et al., 2014
7	Luojiang/ Hemudu	AD 955-8155	2	Y	Hiatus inferred from the radiocarbon age (sedimentation rate: 0.1 mm yr^{-1})	Pollen	–	Qin et al., 2011
8	Wujiangbang	5435–6145	0	N	N	Pollen	–	Qin et al., 2011
9	Qingpu	AD 170–3710	1	Y	Y	Pollen	Increase in local water level[†]	Itzstein-Davey et al., 2007
10	Guangfulin[‡]	AD 860–4360	1	Y	Y	Pollen	Increase in local water level[§] and increase in saline biota (Chenopodiaceae)	Chen, 2002; Atahan et al., 2008; Wang et al., 2012
11	Siqian	4290–6160	0	N	N	Diatom	–	Zong et al., 2011
12	Tinglin	4640–6250	0	N	N	Diatom, rice phytoliths	–	Zong et al., 2011
13	Longnan	2860–3580	1	Y	Y	Pollen	Increase in local water level	Zong et al., 2012
14	Yuanjiadi	1920–4430	0	Y	Y	Pollen	Increase in local water level	Zong et al., 2012

15	Guoyuancun	1770−1850	0	N	N	Pollen	–	Zong et al., 2012
16	Tianyilu	390−2080	0	N	N	Pollen	–	Zong et al., 2012
17	Caoxieshan	1180−2790	1	Y	Y	Pollen	Increase in local water level¶	Zong et al., 2012
18	Chuodun	10−1440	0	N	N	Pollen	–	Zong et al., 2012
19	Liangzhu	1120−5605	0	Uncertain due to no age constrain	Y	Pollen	Increase in saline biota (Chenopodiaceae)	Li et al., 2010

* The name "Tangcunmiao" in the original paper should be "Tangmiaocun".

† Age-depth model determined by excluding results from old carbon. Increase in local water level is inferred from the increase in abundance of *Typha* and *Triglochin*-*Potamogeton* type and a decrease in *Artemisia*.

‡ There are two profiles at this site, one from Atahan et al. (2008) and the other (profile-1999) from Chen (2002).

§ Age-depth model of profile in Atahan et al. (2008) was determined by excluding results from old carbon (Wang et al., 2012). Increase in local water level is inferred from the increase in *Typha* abundance in both profiles. Increase in saline biota (Chenopodiaceae) abundance is seen in profile-1999 by Chen (2002).

¶ End of Liangzhu period is inferred from the abrupt decline in abundance of cultural NPPs at 0.6 m (their Figure 6a in Zong et al., 2012). Increase in local water level is inferred from the increase in abundance of open freshwater NPPs.

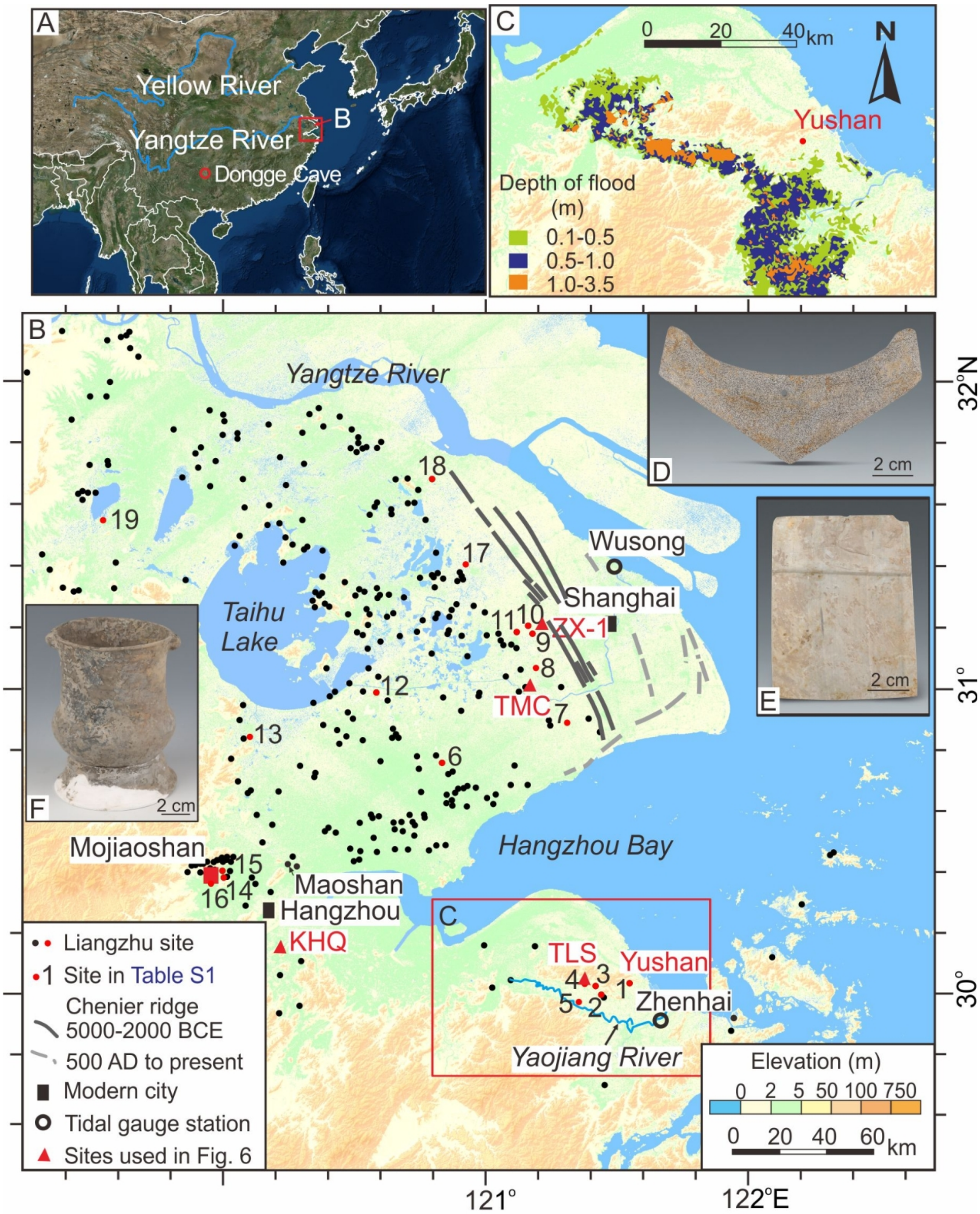

A
Yellow River
Yangtze River
B
Dongge Cave
C
0 20 40 km
N
Yushan
Depth of flood (m)
0.1-0.5
0.5-1.0
1.0-3.5
B
Yangtze River
Taihu Lake
Wusong
Shanghai
ZX-1
TMC
Hangzhou Bay
Mojiaoshan
Maoshan
Hangzhou
KHQ
TLS
Yushan
Zhenhai
Yaojiang River
D
2 cm
E
2 cm
F
2 cm
Liangzhu site
1 Site in Table S1
Chenier ridge 5000-2000 BCE
500 AD to present
Modern city
Tidal gauge station
Sites used in Fig. 6
Elevation (m)
0 2 5 50 100 750
0 20 40 60 km
32°N
31°
30°
121°
122°E

Figure 1

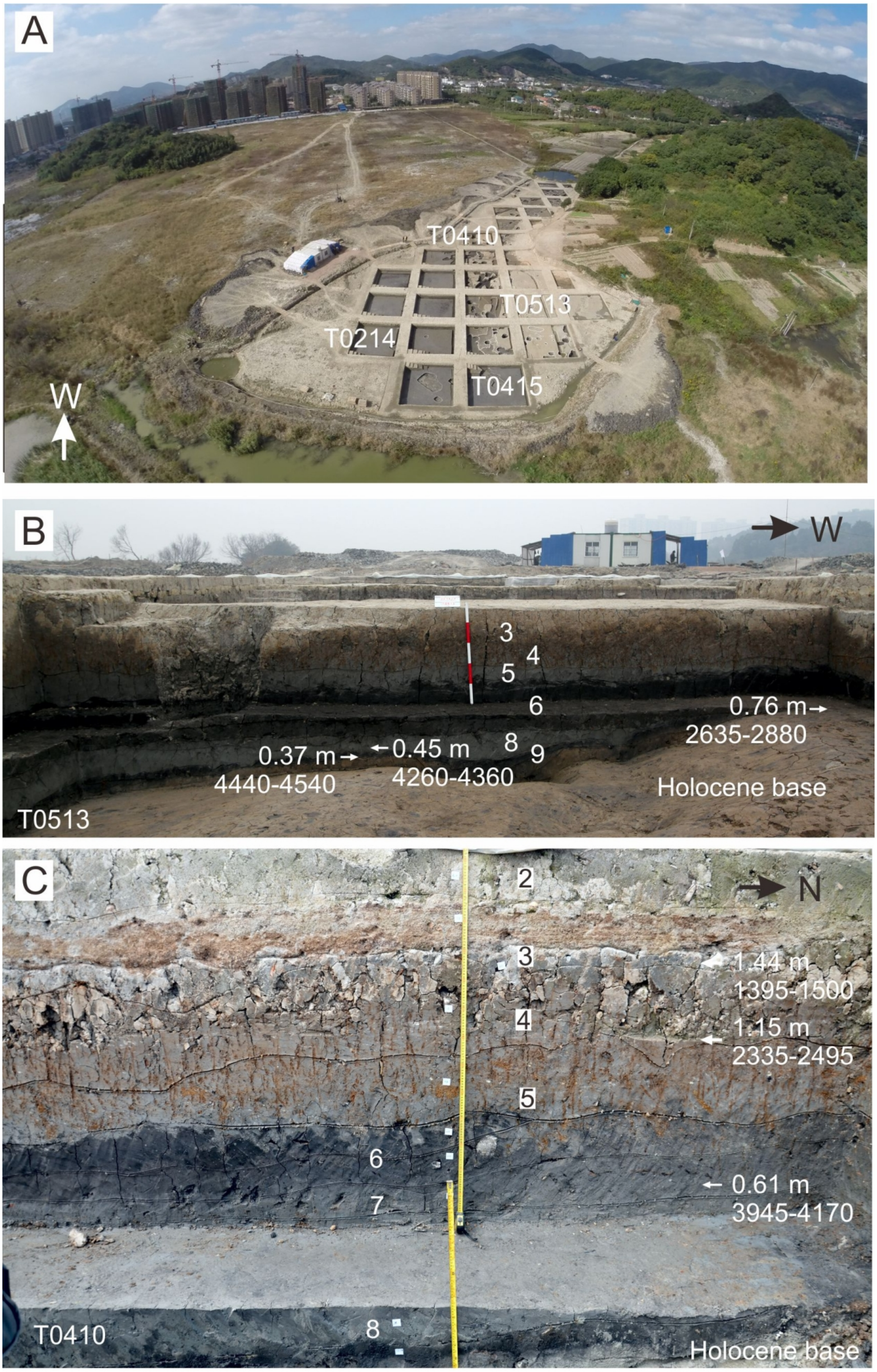
A
T0410
T0513
T0214
T0415
W
B
W
3
4
5
6
0.76 m
2635-2880
8
9
0.37 m
4440-4540
0.45 m
4260-4360
Holocene base
T0513
C
2
N
3
1.44 m
1395-1500
4
1.15 m
2335-2495
5
6
7
0.61 m
3945-4170
T0410
8
Holocene base

Figure 2

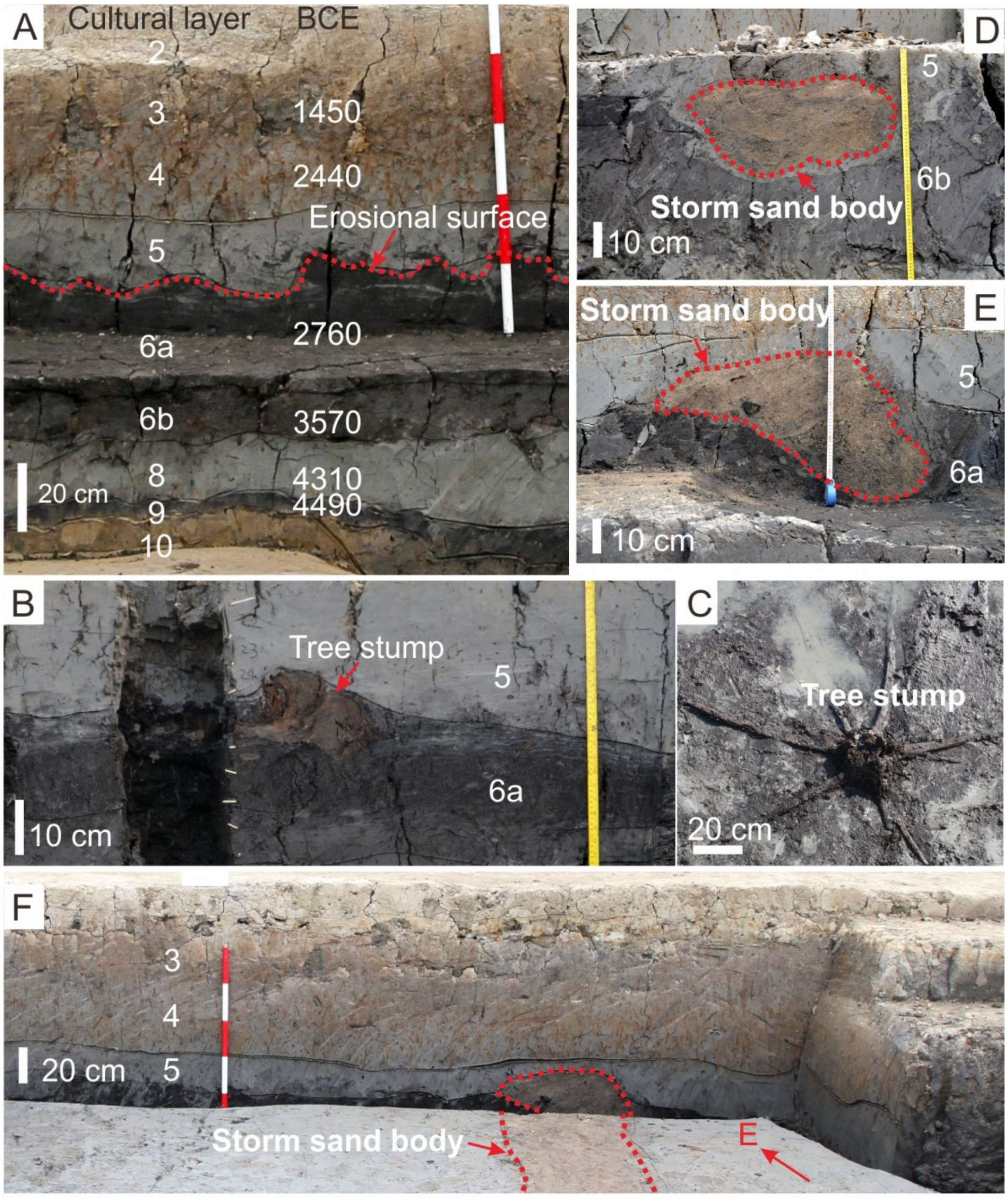

A
Cultural layer
BCE
2
3
1450
4
2440
Erosional surface
5
6a
2760
6b
3570
8
4310
9
4490
10
20 cm
D
5
6b
Storm sand body
10 cm
E
Storm sand body
5
6a
10 cm
B
Tree stump
5
6a
10 cm
C
Tree stump
20 cm
F
3
4
5
20 cm
Storm sand body
E

Figure 3

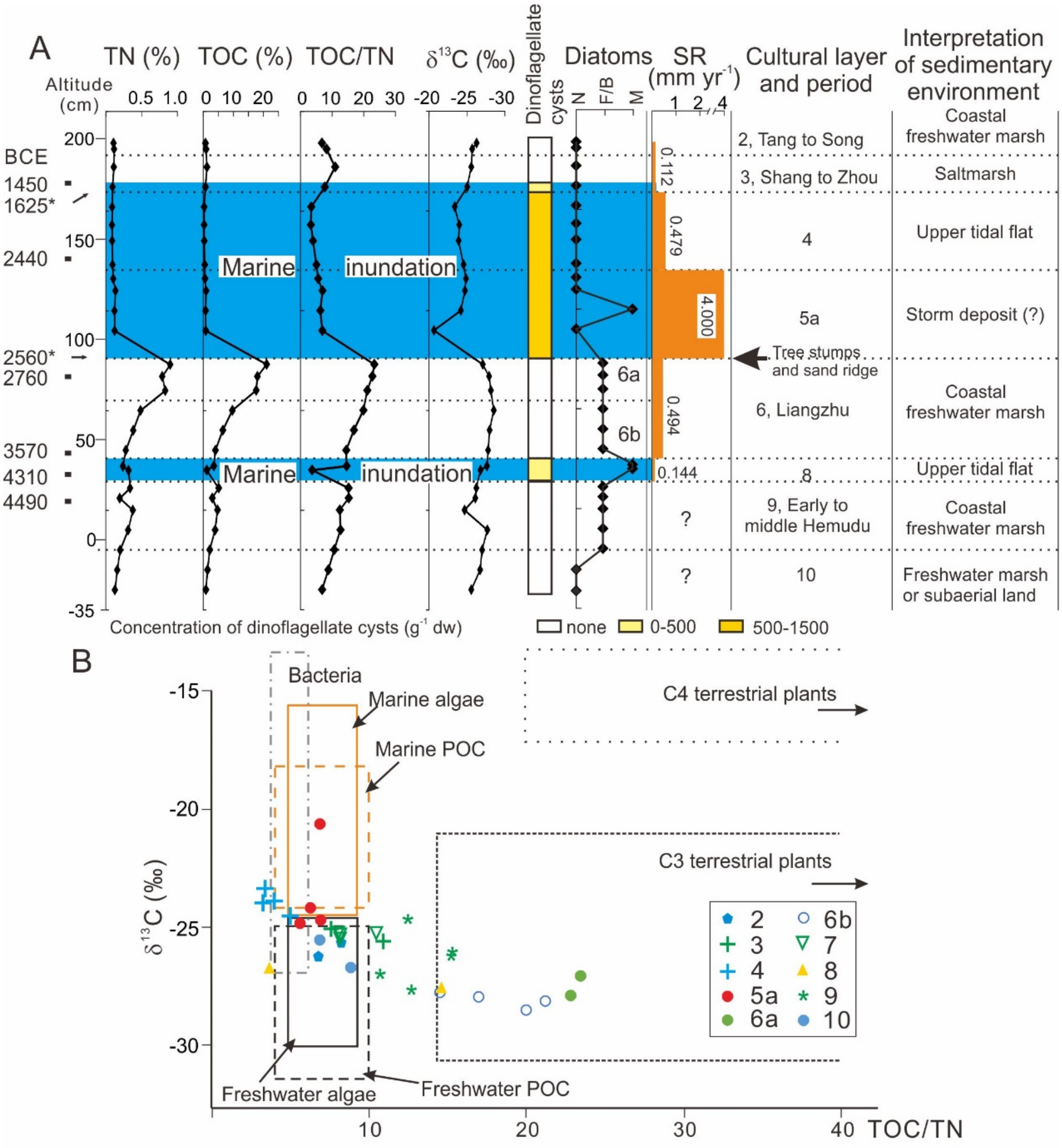

A
TN (%)
TOC (%)
TOC/TN
δ13C (‰)
Dinoflagellate cysts
Diatoms
SR (mm yr-1)
Cultural layer and period
Interpretation of sedimentary environment
Altitude (cm)
BCE
Marine inundation
Tree stumps and sand ridge
2, Tang to Song
3, Shang to Zhou
4
5a
6, Liangzhu
8
9, Early to middle Hemudu
10
Coastal freshwater marsh
Saltmarsh
Upper tidal flat
Storm deposit (?)
Coastal freshwater marsh
Upper tidal flat
Coastal freshwater marsh
Freshwater marsh or subaerial land
Concentration of dinoflagellate cysts (g-1 dw)
none
0-500
500-1500
B
Bacteria
Marine algae
Marine POC
C4 terrestrial plants
C3 terrestrial plants
Freshwater algae
Freshwater POC
δ13C (‰)
TOC/TN

Figure 4

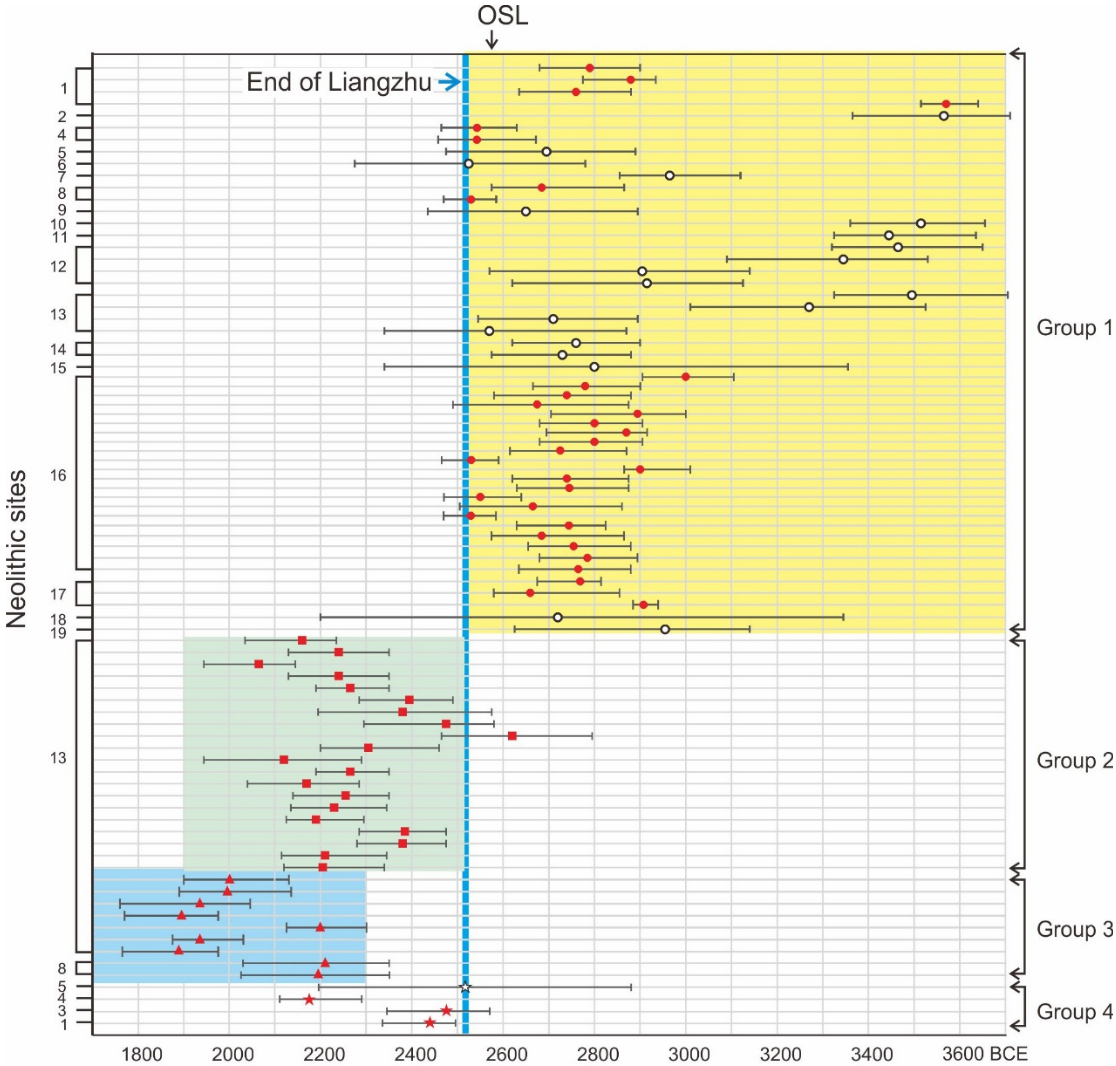

OSL
End of Liangzhu
Neolithic sites
1
2
4
5
6
7
8
9
10
11
12
13
14
15
16
17
18
19
13
8
5
4
3
1
Group 1
Group 2
Group 3
Group 4
1800
2000
2200
2400
2600
2800
3000
3200
3400
3600 BCE

Figure 5

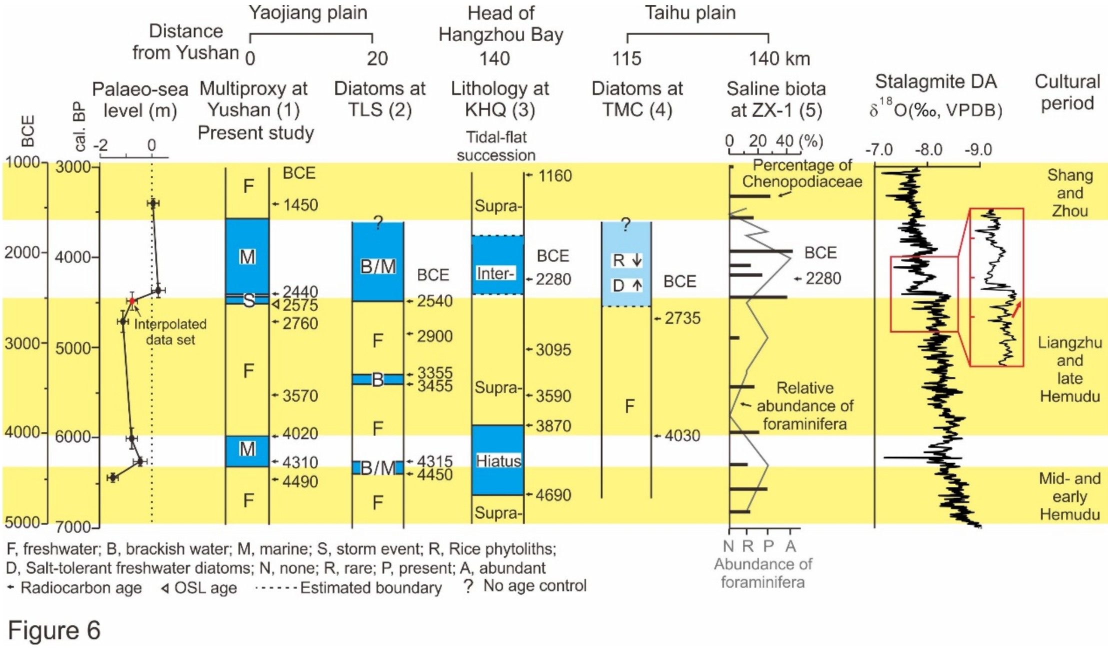

Yaojiang plain
Head of Hangzhou Bay
Taihu plain
Distance from Yushan
0
20
140
115
140 km
Palaeo-sea level (m)
Multiproxy at Yushan (1) Present study
Diatoms at TLS (2)
Lithology at KHQ (3)
Tidal-flat succession
Diatoms at TMC (4)
Saline biota at ZX-1 (5)
Stalagmite DA δ18O(‰, VPDB)
Cultural period
BCE
cal. BP
Interpolated data set
Percentage of Chenopodiaceae
Relative abundance of foraminifera
Supra-
Inter-
Hiatus
Shang and Zhou
Liangzhu and late Hemudu
Mid- and early Hemudu
F, freshwater; B, brackish water; M, marine; S, storm event; R, Rice phytoliths;
D, Salt-tolerant freshwater diatoms; N, none; R, rare; P, present; A, abundant
Radiocarbon age
OSL age
Estimated boundary
? No age control
Abundance of foraminifera

Figure 6

Supplementary Materials for

Mid-Holocene abrupt sea-level rise and human response in the East China coastal plain

Zhanghua Wang[1]*, David B. Ryves[2], Shao Lei[3], Xiaomei Nian[1], Ye Lv[1], Liang Tang[1], Long Wang[1], Jiehua Wang[3], Jie Chen[4]

[1]State Key Laboratory of Estuarine and Coastal Research, ECNU, Shanghai 200062, China.

[2]Centre for Hydrological and Ecosystem Science (CHES), Department of Geography, Loughborough University, Loughborough LE11 3TU, UK.

[3]Ningbo Municipal Institute of Cultural Relics and Archaeology, Ningbo, China.

[4]Shanghai Museum, Shanghai 200003, China.

correspondence to: zhwang@geo.ecnu.edu.cn

This file includes:

Tables S1 to S2
Figs. S1 to S2
References

Table S1 Neolithic sites (seeing Fig. 1 for their location) with 85 radiocarbon ages during and post the Liangzhu period, which we collected from all publications. Radiocarbon ages were recalibrated with the programme Calib 7.1, using a ^{14}C half-life of 5568 years. This work is to revise the time span of the Liangzhu culture and results show that it ended at ~2500 BCE (Fig. 5).

Number in S.I. Fig. 1	Name of site	Cultural layer	Dating material	Radiocarbon age (BP)	2 sigma Calibrated BCE	Prob.	Median prob. (cal. BCE)	Data source	Dating method
1	Yushan	Natural deposit above Liangzhu layer	Plant fragment	3940±30	2335–2495	0.900	2440	Present study	AMS ^{14}C
3	Fujiashan	Natural deposit above Liangzhu layer	Peaty mud	3955±35	2345–2570	1.000	2475	[1]	AMS ^{14}C
4	Tianluoshan	Natural deposit above the rice field	Plant fragment	3760±40	2110–2290	0.813	2175	[2]	AMS ^{14}C
5	Xiangjiashan	Disturbed layer above the Liangzhu	Wood	3990±130	2195–2880	0.986	2515	[3]	Radiometric
8	Guangfulin	Guangfulin	–	3770±60	2025–2350	0.947	2195	[4]	AMS ^{14}C
8	Guangfulin	Guangfulin	–	3780±60	2030–2350	0.925	2210	[4]	AMS ^{14}C
13	Qianshanyang	Guangfulin	Wood	3545±35	1765–1975	0.994	1890	[5]	AMS ^{14}C
13	Qianshanyang	Guangfulin	Charcoal	3580±35	1875–2030	0.944	1935	[5]	AMS ^{14}C
13	Qianshanyang	Guangfulin	Charcoal	3775±35	2125–2300	0.922	2200	[5]	AMS ^{14}C
13	Qianshanyang	Guangfulin	Rice	3550±35	1770–1975	0.983	1895	[5]	AMS ^{14}C
13	Qianshanyang	Guangfulin	Seed	3580±55	1760–2045	0.962	1935	[5]	AMS ^{14}C
13	Qianshanyang	Guangfulin	Charcoal	3630±40	1890–2135	1	1995	[5]	AMS ^{14}C
13	Qianshanyang	Guangfulin	Bone	3635±35	1900–2130	1	2000	[5]	AMS ^{14}C

13	Qianshanyang	Qianshanyang	Charcoal	3780±40	2120–2340	0.919	2205	[5]	AMS ^{14}C
13	Qianshanyang	Qianshanyang	Charcoal	3780±45	2115–2345	0.886	2210	[5]	AMS ^{14}C
13	Qianshanyang	Qianshanyang	Charred bamboo	3895±40	2280–2475	0.965	2380	[5]	AMS ^{14}C
13	Qianshanyang	Qianshanyang	Charred bamboo	3895±35	2285–2475	0.992	2385	[5]	AMS ^{14}C
13	Qianshanyang	Qianshanyang	Charcoal	3770±35	2125–2295	0.900	2190	[5]	AMS ^{14}C
13	Qianshanyang	Qianshanyang	Charcoal	3795±35	2135–2345	0.982	2230	[5]	AMS ^{14}C
13	Qianshanyang	Qianshanyang	Wood	3815±35	2140–2350	0.934	2255	[5]	AMS ^{14}C
13	Qianshanyang	Qianshanyang	Bamboo	3755±35	2040–2285	1.000	2170	[5]	AMS ^{14}C
13	Qianshanyang	Qianshanyang	Bamboo	3820±35	2190–2350	0.828	2265	[5]	AMS ^{14}C
13	Qianshanyang	Qianshanyang	Rice	3720±60	1945–2290	1.000	2120	[5]	AMS ^{14}C
13	Qianshanyang	Qianshanyang	Seed	3840±40	2200–2460	0.991	2305	[5]	AMS ^{14}C
13	Qianshanyang	Qianshanyang	Seed	4060±70	2465–2795	0.845	2620	[5]	AMS ^{14}C
13	Qianshanyang	Qianshanyang	Plant fiber	3960±50	2295–2580	1.000	2475	[5]	AMS ^{14}C
13	Qianshanyang	Qianshanyang	Seed	3905±75	2195–2575	0.982	2380	[5]	AMS ^{14}C
13	Qianshanyang	Qianshanyang	Bone	3910±40	2285–2490	0.980	2395	[5]	AMS ^{14}C
13	Qianshanyang	Qianshanyang	Bone	3820±35	2190–2350	0.828	2265	[5]	AMS ^{14}C
13	Qianshanyang	Qianshanyang	Burned earth	3800±40	2130–2350	0.935	2240	[5]	AMS ^{14}C
13	Qianshanyang	Qianshanyang	Bamboo	3675±40	1945–2145	0.960	2065	[5]	AMS ^{14}C
13	Qianshanyang	Qianshanyang	Charcoal	3800±40	2130–2350	0.935	2240	[5]	AMS ^{14}C
13	Qianshanyang	Qianshanyang	Charcoal	3750±40	2035–2235	0.881	2160	[5]	AMS ^{14}C
1	Yushan	Liangzhu	Tree stump	4210±30	2680–2900	1.000	2790	Present study	AMS ^{14}C
1	Yushan	Liangzhu	Tree stump	4240±30	2705–2910	1.000	2880	Present study	AMS ^{14}C
1	Yushan	Liangzhu	Plant fragments	4170±30	2635–2880	1.000	2760	Present study	AMS ^{14}C
1	Yushan	Liangzhu	Organic sediments	4770±30	3515–3640	0.980	3570	Present study	AMS ^{14}C
2	Cihu	Liangzhu	Wood	4790±85	3365–3710	1.000	3565	[6]	Radiometric

4	Tianluoshan	Top of the Neolithic rice field	Seeds	4020±40	2465–2635	0.980	2540	[7]	AMS ^{14}C
4	Tianluoshan	Top of the Neolithic rice field	Seeds	4015±45	2455–2675	0.970	2540	[1]	AMS ^{14}C
5	Xiangjiashan	Liangzhu	Wood	4115±90	2475–2890	1.000	2695	[3]	Radiometric
6	Quemuqiao	Liangzhu	Wood	3995±95	2275–2780	0.905	2525	[8]	Radiometric
7	Tinglin	Liangzhu	Charred wood	4320±70	2855–3120	0.885	2965	[9]	Radiometric
8	Guangfulin	Liangzhu	Organic-rich mud	4110±30	2575–2865	1.000	2685	[10]	AMS ^{14}C
8	Guangfulin	Liangzhu	Organic-rich mud	4020±30	2470–2585	0.959	2530	[10]	AMS ^{14}C
9	Guoyuancun	Liangzhu	Wood	4080±100	2435–2895	0.973	2650	[9]	Radiometric
10	Fuquanshan	Liangzhu	Charred wood	4730±80	3360–3655	1.000	3515	[11]	Radiometric
11	Siqian	Liangzhu	Bamboo	4645±70	3325–3635	0.910	3445	[12]	Radiometric
12	Longnan	Liangzhu	Charcoal	4685±90	3320–3650	0.931	3465	[13]	Radiometric
12	Longnan	Liangzhu	Charcoal	4595±80	3090–3530	0.950	3345	[13]	Radiometric
12	Longnan	Liangzhu	Charcoal	4280±125	2570–3140	0.879	2905	[13]	Radiometric
12	Longnan	Liangzhu	Macrocharcoal	4290±100	2620–3125	0.911	2915	[13]	Radiometric
13	Qianshanyang	Liangzhu	Charred rice	4715±100	3325–3705	0.953	3495	[9]	Radiometric
13	Qianshanyang	Liangzhu	Wood tool	4565±90	3010–3525	0.976	3270	[14]	Radiometric
13	Qianshanyang	Liangzhu	Wood tool	4130±85	2545–2895	0.929	2710	[14]	Radiometric
13	Qianshanyang	Liangzhu	Bamboo	4025±85	2340–2870	0.996	2570	[14]	Radiometric
14	Miaoqian	Late Liangzhu	Charcoal	4184±61	2620–2900	0.975	2760	[15]	Radiometric
14	Miaoqian	Late Liangzhu	Charcoal	4137±54	2575–2880	1.000	2730	[15]	Radiometric
15	Anxi	Liangzhu	Wood	4215±180	2340–3355	0.999	2800	[14]	Radiometric
16	Bianjiashan	Liangzhu	Freshwater gastropod shell	4385±40	2905–3105	0.98	3000	[16]	AMS ^{14}C
16	Bianjiashan	Liangzhu	Plant remains	4200±40	2665–2900	0.98	2780	[16]	AMS ^{14}C

16	Bianjiashan	Liangzhu	Plant remains	4150±55	2580–2880	1	2740	[16]	AMS ^{14}C
16	Bianjiashan	Liangzhu	Plant remains	4095±70	2490–2875	1	2675	[16]	AMS ^{14}C
16	Bianjiashan	Liangzhu	Plant remains	4265±35	2705–3000	1	2895	[16]	AMS ^{14}C
16	Bianjiashan	Liangzhu	Plant remains	4220±35	2680–2905	1	2800	[16]	AMS ^{14}C
16	Bianjiashan	Liangzhu	Plant remains	4235±55	2695–2915	1	2870	[16]	AMS ^{14}C
16	Bianjiashan	Liangzhu	Plant remains	4220±35	2680–2905	1	2800	[16]	AMS ^{14}C
16	Bianjiashan	Liangzhu	Plant remains	4130±40	2615–2870	0.93	2725	[16]	AMS ^{14}C
16	Bianjiashan	Liangzhu	Plant remains	4010±35	2465–2590	0.96	2530	[16]	AMS ^{14}C
16	Bianjiashan	Liangzhu	Plant remains	4275±40	2865–3010	0.92	2900	[16]	AMS ^{14}C
16	Bianjiashan	Liangzhu	Plant remains	4145±35	2620–2875	1	2740	[16]	AMS ^{14}C
16	Bianjiashan	Liangzhu	Ash	4150±30	2630–2875	1	2745	[16]	AMS ^{14}C
16	Bianjiashan	Liangzhu	Ash	4030±40	2470–2640	0.95	2550	[16]	AMS ^{14}C
16	Bianjiashan	Liangzhu	Fabric	4100±30	2505–2860	1	2665	[16]	AMS ^{14}C
16	Bianjiashan	Liangzhu	HyPy residue of charcoal*	4020±30	2470–2585	0.959	2530	[17]	AMS ^{14}C
16	Bianjiashan	Liangzhu	HyPy residue of charcoal	4150±30	2630–2825	0.804	2745	[17]	AMS ^{14}C
16	Bianjiashan	Liangzhu	HyPy residue of charcoal	4110±30	2575–2865	1.000	2685	[17]	AMS ^{14}C
16	Bianjiashan	Liangzhu	HyPy residue of charcoal	4160±30	2655–2880	0.951	2755	[17]	AMS ^{14}C
16	Bianjiashan	Liangzhu	Wood	4200±30	2680–2895	1	2785	[17]	AMS ^{14}C
16	Bianjiashan	Liangzhu	Wood	4170±30	2635–2880	1	2765	[17]	AMS ^{14}C
17	Zhumucun	Liangzhu	Plant	4170±20	2675–2815	0.805	2770	[18]	AMS ^{14}C
17	Zhumucun	Liangzhu	Charred rice grain	4105±20	2580–2855	1.000	2660	[18]	AMS ^{14}C
17	Zhumucun	River channel†	Charred rice grain	3885±25	2295–2465	1.000	2385	[18]	AMS ^{14}C

17	Zhumucun	Liangzhu	Charred rice grain	4305±25	2885–2940	0.925	2910	[18]	AMS ^{14}C
18	Sidun	Liangzhu	Charcoal	4150±205	2200–3345	0.996	2720	[19	Radiometric
19	Yangzhu	Liangzhu	Wood	4310±110	2625–3140	0.849	2955	[20]	Radiometric

* HyPy (catalytic hydropyrolysis) residue is the contaminant-free black carbon fraction of charcoal and thus can produce an accurate ^{14}C age.

† This sample was collected from river channel which could deposit younger sediments, thus it was excluded in Fig. 5.

Table S2 Radiocarbon ages collected from TLS (Tianluoshan), KHQ (Kuahuqiao), TMC (Tangmiaocun) and ZX-1 and their calibration using the Calib 7.1 program. The mollusk shell was calibrated using the Marine13 calibration curve and the regional reservoir correction (ΔR) value of −1±143 was averaged from samples from Tsingtao, southwest coast of Korea and northwest coast of Taiwan[24–26].

Name of site	Dating material	Radiocarbon age (BP)	2 sigma Calibrated BCE	Prob.	Median prob. (cal. BCE)	Data source
TLS	Seeds	4020±40	2465–2635	0.98	2540	[7]
	Seeds	4275±40	2865–3010	0.92	2900	[7]
	Seeds	4585±35	3115–3500	1	3355	[7]
	Seeds	4660±40	3360–3525	0.96	3455	[7]
	Seeds	5465±45	4235–4375	0.96	4315	[7]
	Seeds	5620±35	4360–4520	1	4450	[7]
KHQ	Not given	2950±100	915–1415	1	1160	[21]
	Not given	3825±100	2015–2500	0.97	2280	[21]
	Not given	4410±120	2860–3375	0.96	3095	[21]
	Not given	4820±150	3325–3965	0.97	3590	[21]
	Not given	5070±150	3630–4245	0.96	3870	[21]
	Not given	5820±170	4335–5075	0.99	4690	[21]
TMC	Pollen residue	4140±40	2615–2875	0.97	2735	[22]
	Pollen residue	5230±40	3965–4225	1	4030	[22]
ZX-1	Mollusc shell	4160±40	1870–2695	1	2280	[23]

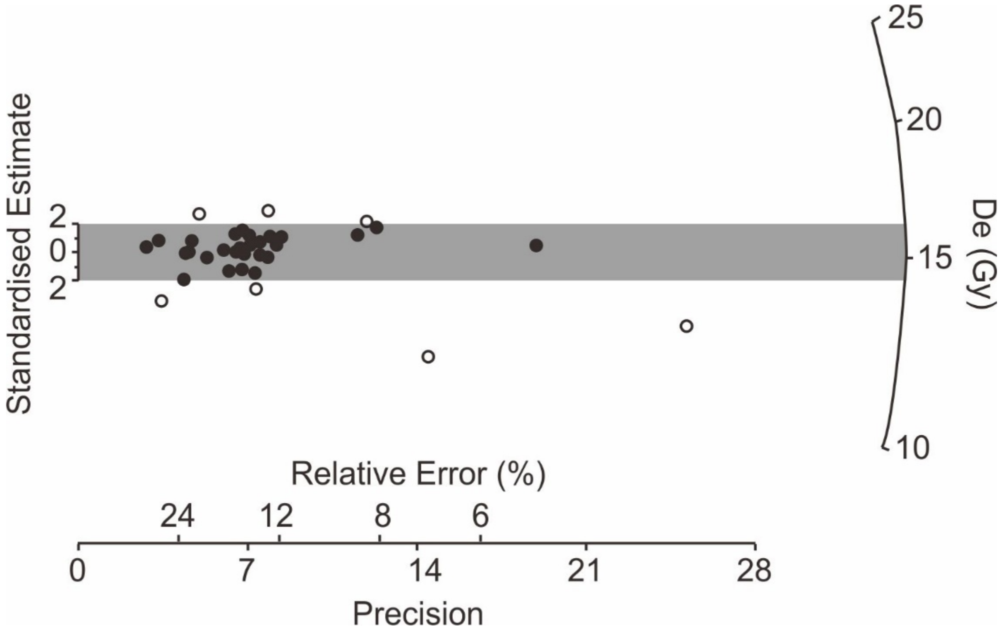

Figure S1 Radial plot of measured doses (Central Age Model, CAM) for single grains of quartz from Yushan site. The open symbols relate to De values outside the ±2δ range.

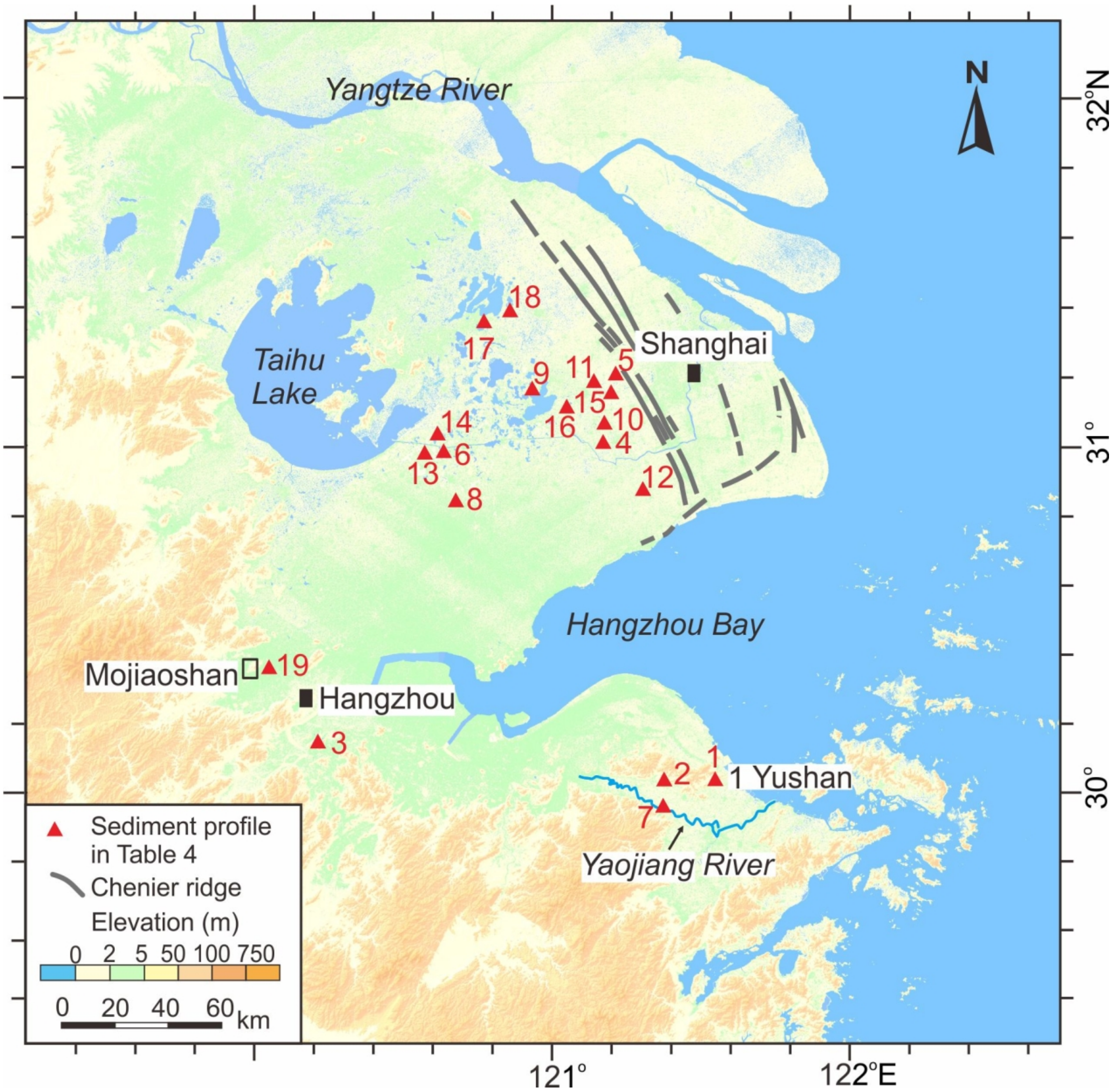

Figure S2 Distribution of sediment profiles with high-resolution radiocarbon dates (Tables 4, S2). The map is generated by software ArcGis 10.1 (www.esrichina.com.cn) using the data set of topography provided by International Scientific & Technical Data Mirror Site, Computer Network Information Center, Chinese Academy of Sciences (http://www.gscloud.cn).

References

1. Zheng, Y., Sun, G., Qin, L., Li, C., Wu, X., Chen, X., 2009. Rice fields and modes of rice cultivation between 5000 and 2500 BC in east China. Journal of Archaeological Science 36, 2609–2616.
2. Ningbo Municipal Institute of Cultural Relics and Archaeology, 2013. FU JIA SHAN——The Excavated Report on the Neolithic Site. Science Press, Beijing (in Chinese).
3. Institute of Archaeology, Chinese Academy of Social Science, 1996. Radiocarbon reports (23). KAO GU (7), 66–70 (in Chinese).
4. Shanghai Museum, 2002. The excavated report on the Neolithic site GUANG FU LIN, Songjiang, Shanghai during 1999-2000. KAO GU (10), 31–48 (in Chinese).
5. Zhejiang Provincial Institute of Cultural Relics and Archaeology, Huzhou Meseum, 2014. Qianshanyang: a report on the third and fourth excavations of the site. WEN WU Press, Beijing (in Chinese).
6. Liu, J., 2006. The Hemudu Culture. WEN WU Press, Beijing (in Chinese).
7. Zheng, Y., Sun, G., Chen, X., 2012. Response of rice cultivation to fluctuating sea level during the Mid-Holocene. Chinese Science Bulletin 57, 370–378.
8. Jiaxing Museum, 1974. The black pottery discovered at Quemuqiao, Jiaxing. KAO GU (4), 249–250 (in Chinese).
9. Institute of Archaeology & Chinese Academy of Social Science, 1992. Radiocarbon database in Chinese Archaeology (1965–1991). WEN WU Press, Beijing (in Chinese).
10. Wang, Z., Chen, J., Zhan, Q., Zhuang, C., Wu, X., Wang, X., 2014. Holocene paleo-

environmental change and its relationship with the Neolithic culture at Guangfulin site. Proceedings on the excavation at Guang Fu Lin, ed. Shanghai Museum (Shanghai Gu Ji Press, Shanghai), pp325–335 (in Chinese).

11. Shanghai Cultural Relics Committee, 2001. FU QUAN SHAN-The excavated report on the Neolithic Site. WEN WU Press, Beijing (in Chinese).
12. Department of Archaeology, Beijing University, 1996. Radiocarbon reports (10). WEN WU (6), 91–95 (in Chinese).
13. Suzhou Museum & Wujiang cultural relics committee, 1990. The report of first and second excavation on the Longnan Neolithic site, Wujiang, Jiangsu. WEN WU (7), 1–27 (in Chinese).
14. Institute of Archaeology, Chinese Academy of Social Science, 1977. Radiocarbon reports. KAO GU (3), 200–204 (in Chinese).
15. Institute of Archaeology, Chinese Academy of Social Science, 1999. Radiocarbon reports (25). KAO GU (7), 80–83 (in Chinese).
16. Zhejiang Provincial Institute of Cultural Relics and Archaeology, 2014. Bianjiashan Site, the Sixth Part Report of Liangzhu Culture Sites. WEN WU Press, Beijing (in Chinese).
17. Zhang, X., Huang, D., Deng, H., Snape, C., Meredit,h W., Zhao, Y., Du, Y., Chen, X., Sun, Y., 2015. Radiocarbon dating of charcoal from the Bianjiashan site in Hangzhou: New evidence for the lower age limit of the Liangzhu Culture. Quaternary Geochronology 30, 9–17.
18. Qiu, Z., Shang, X., Ferguson, D.K., Jiang, H., 2016. Archaeobotanical analysis of diverse plant food resources and palaeovegetation at the Zhumucun site, a late Neolithic settlement

of the Liangzhu Culture in east China. Quaternary International 426, 75–85.

19. Nanjing Museum, 1984. The excavated report on the Sidun Neolithic site, Wujing, Changzhou, Jiangsu in 1982. KAO GU (2), 109–129 (in Chinese).
20. Wu, J., 1988. Distribution of prehistory sites and the environmental change on the Yangtze Delta plain. DONG NAN WEN HUA (6), 16–36 (in Chinese).
21. ZPICRA, 2004. KUA HU QIAO-Archaeological Report of Puyang River Valley I. WEN WU Press, Beijing (in Chinese).
22. Zong, Y., Innes, J.B., Wang, Z., Chen, Z., 2011. Mid-Holocene coastal hydrology and salinity changes in the east Taihu area of the lower Yangtze wetlands, China. Quaternary Research 76, 69–82.
23. Chen, Z., Wang, Z., Schneiderman, J., Cai, Y., 2005. Holocene climate fluctuations on millennium scale in the Yangtze delta of eastern China: implications and response. The Holocene 15, 917–926.
24. Southon, J., Kashgarian, M., Fontugne, M., Metivier, B., Yim, W.W.-S., 2002. Marine reservoir corrections for the Indian Ocean and Southeast Asia. Radiocarbon 44, 167–180.
25. Kong, G.S., Lee, C.W., 2005. Marine reservoir corrections (ΔR) for southern coastal waters of Korea. The Sea, Journal of the Korean Society of Oceanography 10(2), 124–128.
26. Yoneda, M., Uno, H., Shibata, Y., Suzuki, R., Kumamoto, Y., Yoshida, K., Sasaki, T., Suzuki, A., Kawahata, H., 2007. Radiocarbon marine reservoir ages in the western Pacific estimated by pre-bomb molluscan shells. Nuclear Instruments and Methods in Physics Research B 259, 432–437.